Chapter 12
High Resolution Schemes

Abstract This chapter continues the development of convection schemes and discusses approaches by which boundedness is enforced on High Order (HO) convection schemes to produce High Resolution (HR) schemes. The recipe for a HR scheme is shown to involve a combination of a HO profile and a Convection Boundedness Criterion (CBC) ensuring that no oscillatory behavior is experienced in the solution. The Normalized Variable Formulation (NVF) and the Total Variation Diminishing (TVD) frameworks for developing HR schemes are introduced. Even though the two approaches look very different they are shown to be almost identical. The Normalized Variable Diagram (NVD) and Sweby's (or $r-\psi$) diagram for visualizing HR schemes in the NVF and TVD formulation, respectively, are presented. The functional relationships for several HR schemes are specified in the context of both the NVF and TVD formulations. In addition to the Deferred Correction (DC) procedure discussed in the previous chapter, two additional techniques for the implementation of HO and HR schemes in structured and unstructured grids are introduced, namely the Downwind Weighing Factor (DWF) method and the Normalized Weighing Factor (NWF) method.

12.1 The Normalized Variable Formulation (NVF)

The Normalized Variable Formulation (NVF) is a framework for the description and analysis of High Resolution (HR) schemes. It was introduced by Leonard [1–3] and gained popularity with the Gaskell and Lau simplified Convection Boundedness Criterion (CBC) [4]. The Normalized Variable Diagram (NVD) is a useful tool for the development and analysis of HO and HR schemes.

The NVF is a face formulation procedure based on locally normalizing the dependent variable for which the value ϕ_f at face f is to be constructed. The approach relies on the upwind (ϕ_C), downwind (ϕ_D), and far upwind (ϕ_U) node values, illustrated in Fig. 12.1, to express the normalized variable as

F. Moukalled et al., *The Finite Volume Method in Computational Fluid Dynamics*,
Fluid Mechanics and Its Applications 113, DOI 10.1007/978-3-319-16874-6_12

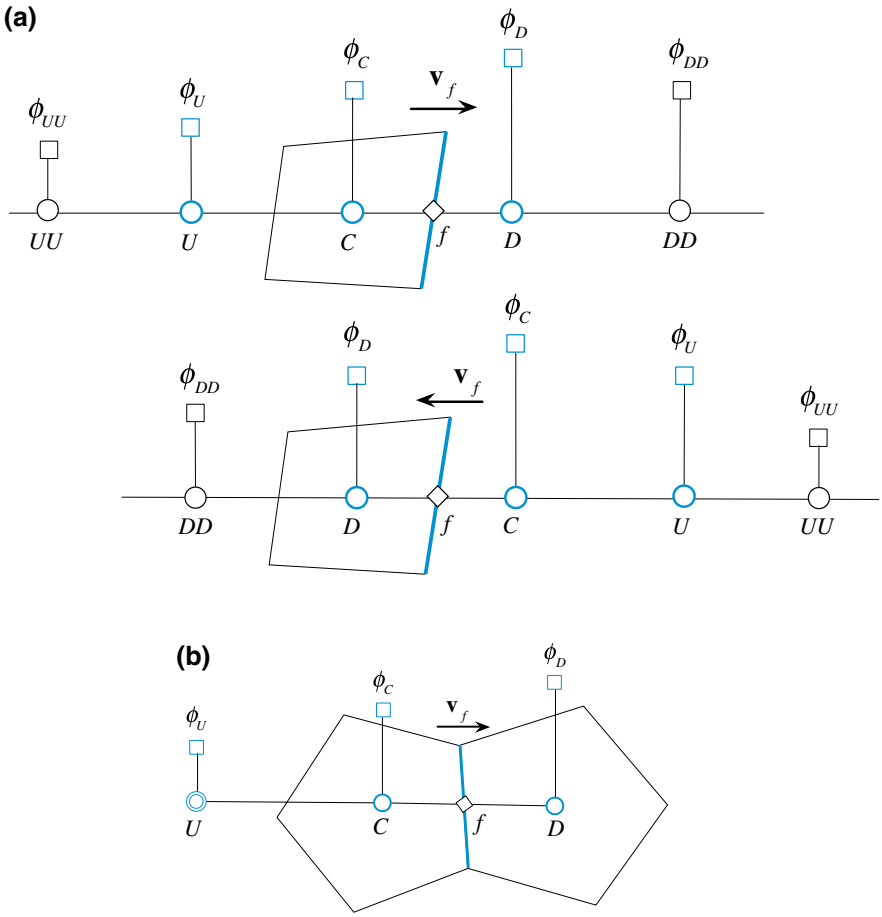

Fig. 12.1 A schematic showing **a** the U, C, and D node locations used in describing convection schemes on structured grids **b** the C, D and extrapolated U nodes for an unstructured grid

$$\tilde{\phi} = \frac{\phi - \phi_U}{\phi_D - \phi_U} \tag{12.1}$$

With this normalization the relation

$$\phi_f = f(\phi_U, \phi_C, \phi_D) \tag{12.2}$$

is transformed to

$$\tilde{\phi}_f = f\left(\tilde{\phi}_C\right) \tag{12.3}$$

since the normalized values of ϕ_D and ϕ_U become equal to

$$\tilde{\phi}_U = 0 \text{ and } \tilde{\phi}_D = 1 \tag{12.4}$$

while the normalized value of $\phi_C\left(\tilde{\phi}_C\right)$ becomes an indicator of smoothness for the ϕ field. Values of $\tilde{\phi}_C$ between 0 and 1 $\left(0<\tilde{\phi}_C<1\right)$, represent a monotonic profile while values of $\tilde{\phi}_C$ that are less than 0 $\left(\tilde{\phi}_C<0\right)$ or greater than 1 $\left(\tilde{\phi}_C>1\right)$ indicate an extremum at C. In addition, values of $\tilde{\phi}_C \approx 0$ or $\tilde{\phi}_C \approx 1$ indicate a gradient jump. These configurations are illustrated in Fig. 12.2.

Normalization is also useful for transforming the functional relationships of HO schemes into linear relations between $\tilde{\phi}_f$ and $\tilde{\phi}_C$. For example, the normalized functional relationships of the HO schemes presented in the previous chapter are as follows:

Upwind: $$\phi_f = \phi_C \quad \Rightarrow \tilde{\phi}_f = \tilde{\phi}_C \tag{12.5}$$

Central difference: $$\phi_f = \frac{1}{2}(\phi_C + \phi_D) \quad \Rightarrow \tilde{\phi}_f = \frac{1}{2}\left(1 + \tilde{\phi}_C\right) \tag{12.6}$$

Second order upwind: $$\phi_f = \frac{3}{2}\phi_C - \frac{1}{2}\phi_U \quad \Rightarrow \tilde{\phi}_f = \frac{3}{2}\tilde{\phi}_C \tag{12.7}$$

FROMM: $$\phi_f = \phi_C + \frac{\phi_D - \phi_U}{4} \quad \Rightarrow \tilde{\phi}_f = \tilde{\phi}_C + \frac{1}{4} \tag{12.8}$$

QUICK: $$\phi_f = \frac{3}{8}\phi_D + \frac{3}{4}\phi_C - \frac{1}{8}\phi_U \quad \Rightarrow \tilde{\phi}_f = \frac{3}{8} + \frac{3}{4}\tilde{\phi}_C \tag{12.9}$$

Downwind: $$\phi_f = \phi_D \quad \Rightarrow \tilde{\phi}_f = 1 \tag{12.10}$$

Thus, for all HO schemes that are based on three nodal values, $\tilde{\phi}_f$ can always be expressed as a linear function of $\tilde{\phi}_C$, i.e., $\tilde{\phi}_f = \ell\tilde{\phi}_C + k$, where the values of ℓ and k depend on the scheme. Therefore, if $\tilde{\phi}_f$ is plotted as a function of $\tilde{\phi}_C$ in the $\left(\tilde{\phi}_C, \tilde{\phi}_f\right)$ plane, then the functional relationships of these schemes will appear as straight lines on the plot. The resultant plot is denoted by the Normalized Variable Diagram (NVD). An NVD on which the functional relationships of the above schemes are plotted is displayed in Fig. 12.3.

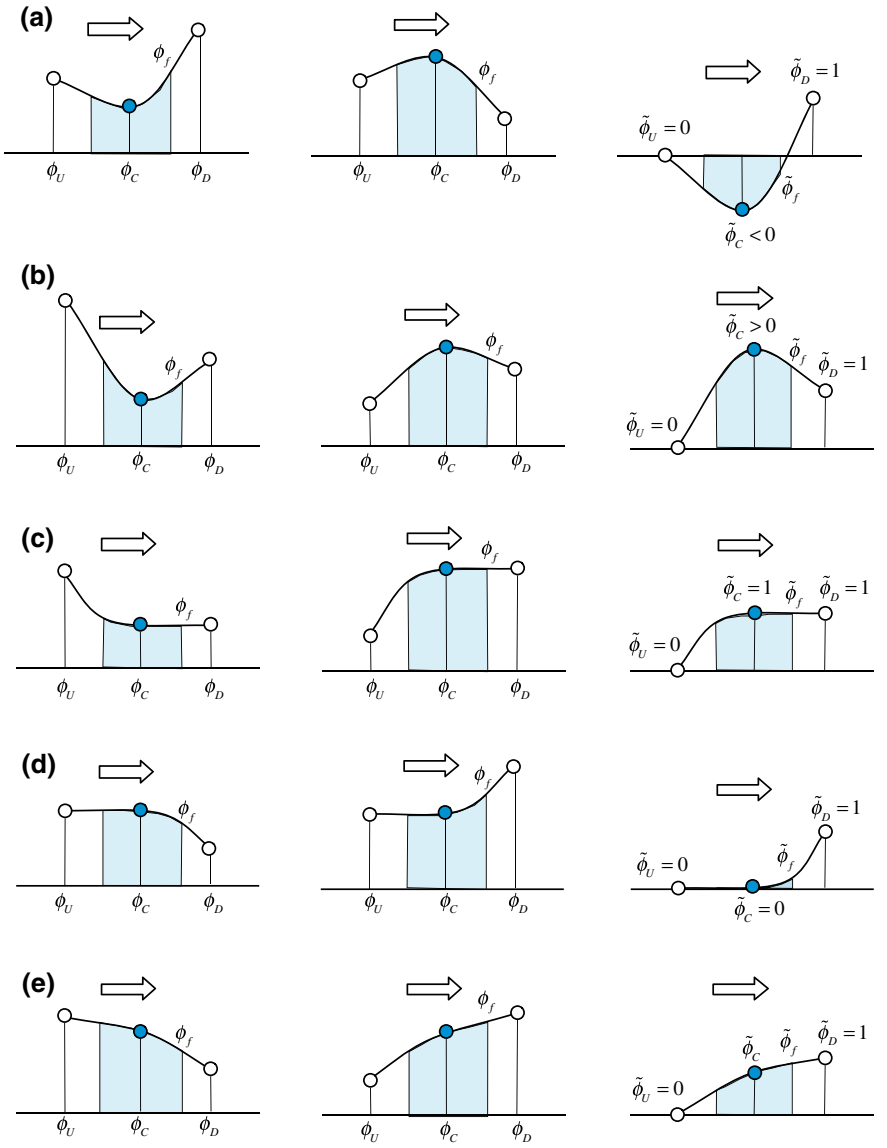

Fig. 12.2 Schematics of the situations when **a** $\tilde{\phi}_C < 0$, **b** $\tilde{\phi}_C > 1$, **c** $\tilde{\phi}_C = 1$, **d** $\tilde{\phi}_C = 0$, and **e** $0 < \tilde{\phi}_C < 1$

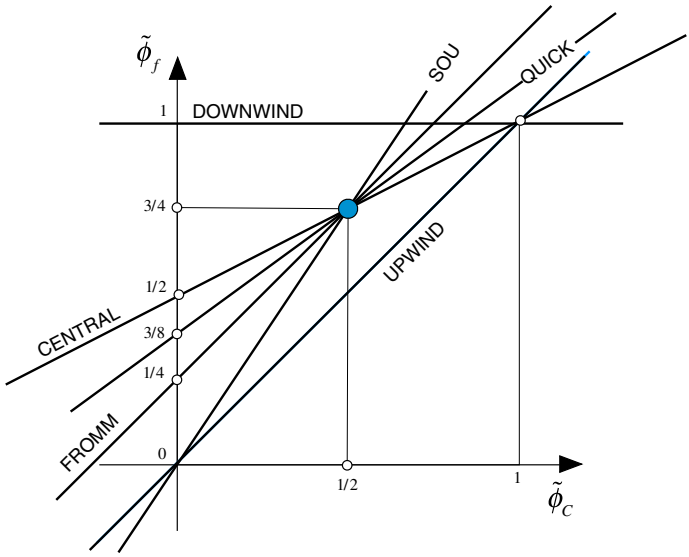

Fig. 12.3 Some HO schemes written in normalized form and plotted on a Normalized Variable Diagram (NVD)

Example 1
Derive the NVF form of the QUICK scheme.

Solution
Starting with

$$\phi_f = \frac{3}{8}\phi_D + \frac{3}{4}\phi_C - \frac{1}{8}\phi_U$$

Applying normalization to both sides yields

$$\frac{\phi_f - \phi_U}{\phi_D - \phi_U} = \frac{\left(\frac{3}{8}\phi_D + \frac{3}{4}\phi_C - \frac{1}{8}\phi_U\right) - \phi_U}{\phi_D - \phi_U}$$

noting that

$$\frac{3}{8} + \frac{3}{4} - \frac{1}{8} = \frac{3}{8} + \frac{6}{8} - \frac{1}{8} = \frac{8}{8} = 1$$

the following is obtained:

$$\frac{\phi_f - \phi_U}{(\phi_D - \phi_U)} = \frac{\frac{3}{8}(\phi_D - \phi_U) + \frac{3}{4}(\phi_C - \phi_U) - \frac{1}{8}(\phi_U - \phi_U)}{(\phi_D - \phi_U)}$$
$$= \frac{3}{8} + \frac{3}{4}\left(\frac{\phi_C - \phi_U}{\phi_D - \phi_U}\right)$$

thus

$$\tilde{\phi}_f = \frac{3}{8} + \frac{3}{4}\tilde{\phi}_C$$

The NVD reveals that except for the first order upwind and downwind schemes, all second order and third order schemes pass through the point $Q(0.5, 0.75)$ (for uniform grids). In fact, it can be shown that for a scheme to be second order accurate it has to pass through Q. If, in addition, its slope at Q is 0.75 then it will be third order accurate (e.g., QUICK). The upwind scheme was shown to be very diffusive, while the downwind scheme very compressive (anti-diffusive). Therefore, from the NVD it can graphically be deduced that any scheme whose functional relationship is close to the upwind scheme is diffusive while anyone close to the downwind scheme is compressive.

Example 2
Show that for schemes developed over uniform cartesian grids to be second order accurate their functional relationships should pass through the point $Q(1/2, 3/4)$ *in the NVD.*

Solution
Second order schemes involve three points. Expanding ϕ_C, ϕ_U, and ϕ_D in terms of ϕ_f, the following is obtained:

$$\phi_C = \phi_f - \frac{1}{2}\Delta x\phi'_f + O(\Delta x^2)$$
$$\phi_U = \phi_f - \frac{3}{2}\Delta x\phi'_f + O(\Delta x^2)$$
$$\phi_D = \phi_f + \frac{1}{2}\Delta x\phi'_f + O(\Delta x^2)$$

The value of ϕ_f is generally obtained as a combination of the values at the three locations as

$$a\phi_C + b\phi_U + c\phi_D = (a + b + c)\phi_f + \left(-\frac{1}{2}a - \frac{3}{2}b + \frac{1}{2}c\right)\Delta x\phi'_f + O(\Delta x^2)$$

The value of ϕ_f will be second order accurate if

$$\left(-\frac{1}{2}a-\frac{3}{2}b+\frac{1}{2}c\right)=0\Rightarrow b=\frac{c-a}{3}$$

A first order approximation of ϕ_f is obtained as

$$\begin{aligned}(a+b+c)\phi_f &= a\phi_C+b\phi_U+c\phi_D\Rightarrow \phi_f\\ &=\frac{a}{(a+b+c)}\phi_C+\frac{b}{(a+b+c)}\phi_U\\ &\quad+\frac{c}{(a+b+c)}\phi_D\\ &\Rightarrow (a+b+c)\tilde{\phi}_f=a\tilde{\phi}_C+c\end{aligned}$$

For the above approximation to be second order accurate the following should be true:

$$\left(a+\frac{c-a}{3}+c\right)\tilde{\phi}_f=a\tilde{\phi}_C+c\Rightarrow\left(\frac{2a+4c}{3}\right)\tilde{\phi}_f=a\tilde{\phi}_C+c$$

The above equality will be satisfied for any value of a and c, and consequently any second order scheme, when $\tilde{\phi}_f=3/4$ and $\tilde{\phi}_C=1/2$, in which case

$$\left(\frac{2a+4c}{3}\right)\tilde{\phi}_f=a\tilde{\phi}_C+c\Rightarrow\left(\frac{2a+4c}{3}\right)\frac{3}{4}=\frac{1}{2}a+c\Rightarrow\frac{1}{2}a+c=\frac{1}{2}a+c$$

Therefore all second order schemes pass through the point $Q(1/2,\,3/4)$.

The HO schemes presented in the previous chapter were shown to drastically decrease the truncation error suffered by the first order upwind scheme, while remaining stable. Still, one of the main shortcomings of these schemes is their unboundedness, i.e., their tendency to produce under/overshoots and even oscillations near sudden jumps or steep gradients in the convected variable (see Figs. 11.14b and 11.17). While in some applications small overshoots and/or oscillations may be tolerable, in others, they can lead to catastrophic results, such as in turbulent flow calculations where the convected variable can be the viscosity coefficient.

This oscillatory behavior near steep gradients characterizes all HO linear convective schemes. In fact these schemes are not monotonous in the sense that they produce local maxima and/or minima, i.e., they are not extrema preserving. For a scheme to be extrema preserving, maxima in the solution must be non-increasing and minima non-decreasing (the scheme should not produce over/under shoots). In fact it

was demonstrated by Godunov and Ryabenki [5] that any linear numerical scheme that is monotone can be at most first-order accurate. This implies that all higher order linear schemes cannot be monotonicity preserving, and that to construct monotonicity preserving schemes, non-linear limiter functions should be used. With this understanding, work on developing high order oscillation-free convection schemes resulted in several techniques [6–10] that can be grouped under two categories. In the first approach [11–13] a limited anti-diffusive flux is added to a first-order upwind scheme in such a way that the resulting scheme is capable of resolving sharp gradients without oscillations. In the second category, a smoothing diffusive flux is introduced into an unbounded HO scheme to damp unphysical oscillations [14–17].

Due to their multi-step nature and the difficulty in balancing the two fluxes, flux blending techniques tend to be very expensive numerically. This is why in this book two approaches for developing HR schemes falling under the flux limiter method will be presented. The first follows a composite procedure whereby high order schemes are combined with bounded low order ones, with the switch between them being controlled by a certain criterion [18]. The second method is based on adding to a diffusive first order upwind term an anti-diffusive flux multiplied by a flux limiter. In this case, the resulting HR schemes are also denoted by Total Variational Diminishing (TVD) schemes as explained in a later section.

The composite schemes approach will be presented first within the framework of the Normalized Variable Formulation (NVF) and will be visualized on a Normalized Variable Diagram (NVD). Therefore the NVF and NVD are first described. The use of the NVD will be instrumental for the definition of a criterion that ensures the boundedness of any high order interpolation scheme.

12.2 The Convection Boundedness Criterion (CBC)

A numerical scheme is expected to preserve the physical properties of the phenomenon it is trying to describe or approximate. Therefore the conditions that a bounded convection scheme should satisfy can best be understood by analyzing the physical properties of convection. Since convection transports fluid properties from upstream to downstream, then approximation to convection should possess this transportive attribute. Thus, numerical convection schemes should be upwind biased or else they will lack the convective stability. Therefore in addition to the values at the nodes straddling the interface ϕ_C and ϕ_D, the value at the far upwind node, i.e., ϕ_U, is also important in analyzing advective schemes. Values at nodes farther away are less important. In the NVF presented above, values are normalized such that the effect of ϕ_U is also considered. This is extremely useful as it helps identifying the conditions for which the numerical convection scheme is monotone. Whereas Spekreise's [19] and Barth and Jespersen [20] definition of a monotone scheme (or bounded scheme) involves all neighbors surrounding the face, Leonard [21] and Gaskel and Lau [4] based their definition of monotonicity only on the neighboring points along the local coordinate system such that

$$\min(\phi_C, \phi_D) \leq \phi_f \leq \max(\phi_C, \phi_D) \tag{12.11}$$

Normalizing, the above condition becomes

$$\min\left(\tilde{\phi}_C, 1\right) \leq \tilde{\phi}_f \leq \max\left(\tilde{\phi}_C, 1\right) \tag{12.12}$$

The Convection Boundedness Criterion (CBC) for implicit steady state flow calculation developed by Gaskell and Lau states that for a scheme to have the boundedness property its functional relationship should be continuous, should be bounded from below by $\tilde{\phi}_C$ and from above by unity, and should pass through the points (0, 0) and (1, 1), in the monotonic range $\left(0 < \tilde{\phi}_C < 1\right)$, and for $\tilde{\phi}_C > 1$ or $\tilde{\phi}_C < 0$, the functional relationship $f\left(\tilde{\phi}_C\right)$ should be equal to $\tilde{\phi}_C$. The above conditions illustrated on an NVD in Fig. 12.4, can be mathematically formulated as

$$\tilde{\phi}_f = \begin{cases} f\left(\tilde{\phi}_C\right) & \textit{continuous} \\ f\left(\tilde{\phi}_C\right) = 1 & \textit{if } \tilde{\phi}_C = 1 \\ f\left(\tilde{\phi}_C\right) \textit{ with } \tilde{\phi}_C < f\left(\tilde{\phi}_C\right) < 1 & \textit{if } 0 < \tilde{\phi}_C < 1 \\ f\left(\tilde{\phi}_C\right) = 0 & \textit{if } \tilde{\phi}_C = 0 \\ f\left(\tilde{\phi}_C\right) = \tilde{\phi}_C & \textit{if } \tilde{\phi}_C < 0 \textit{ or } \tilde{\phi}_C > 1 \end{cases} \tag{12.13}$$

The Convection Boundedness Criterion is quite intuitive and can be interpreted by referring to Figs. 12.4 and 12.5. When ϕ_C is in a monotonic profile the interpolation profile at the cell surface should not yield any new extremum. Thus it is constrained by the ϕ values at the nodes straddling the face. As the value of ϕ_C get closer to ϕ_D while still in the monotonic regime, the value of ϕ_f will also tend toward ϕ_D. When ϕ_C becomes equal to ϕ_D, then ϕ_f also becomes equal to ϕ_D and

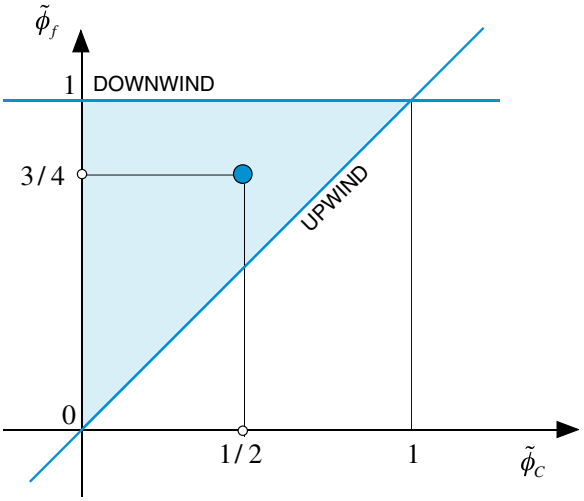

Fig. 12.4 The Convection Boundedness Criterion (CBC) on an NVD Diagram showing the region where $\tilde{\phi}_f$ is bounded

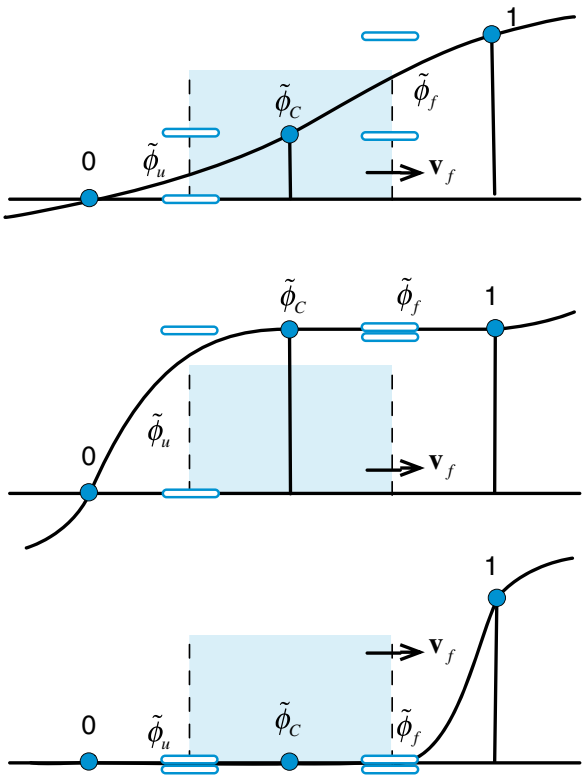

Fig. 12.5 Values of $\tilde{\phi}_f$ and the Convection Boundedness Criterion

thus the condition that $\left(\tilde{\phi}_C, \tilde{\phi}_f\right)$ passes through the point (1, 1). When the value of ϕ_C is such that $\tilde{\phi}_C > 1$, ϕ_f is assigned the upwind value, i.e., ϕ_C. This has the effect of yielding the largest outflow condition possible while fulfilling the condition that ϕ_f is bounded by the nodes straddling the cell face. This behavior means that any undue oscillation will be damped since ϕ_C will tend to a lower value because outflow is larger than inflow in these conditions.

Therefore if there is no external physical mechanism to yield the extrema (a source term for example) the extrema will die out. A similar mechanism takes place when $\tilde{\phi}_C < 0$. However as ϕ_C gets closer to ϕ_U coming from the non-monotonic region, ϕ_f will be equal to the upwind value ϕ_C until $\phi_C = \phi_U$ implying the condition that the profile of ϕ_f passes through the point (0, 0). When $\tilde{\phi}_C < 0$ or $\tilde{\phi}_C > 1$ the solution will be in a region where convection is dominant and the upwind approximation will be an excellent one.

12.3 High Resolution (HR) Schemes

Constructing a bounded HO scheme, i.e., a HR scheme, using the NVD is relatively a simple exercise. Any high order base scheme can be bounded using an ad-hoc set of curves.

To construct a HR scheme, the monotonic profile in the range $0 \le \tilde{\phi}_C \le 1$ should pass through the points (0, 0) and (1, 1), while remaining within the upper triangular shaded region on the NVD (Fig. 12.4). On the other hand, in the non-monotonic range, i.e., $\tilde{\phi}_C < 0$ and/or $\tilde{\phi}_C > 1$, the profile should follow the upwind profile. A number of well-known High-Resolution schemes built in this manner are illustrated in Fig. 12.6.

For improved convergence behavior, any composite HR scheme should avoid hard angles at its profile connection points as well as at its horizontal and vertical profiles. For example with the SMART scheme, which is constructed using the QUICK scheme, the convergence can be substantially improved by a minor modification to the vertical portion of its composite profile using $\tilde{\phi}_f = 3\tilde{\phi}_C$ in the region $0 \le \tilde{\phi}_C \le 1/6$. For the STOIC schemes the modification is applied in the $0 \le \tilde{\phi}_C \le 1/5$ region. Also the horizontal portion of the composite profile for both SMART and STOIC may be slightly modified to further improve convergence. For example, one such modification is to impose a linear profile for $9/10 \le \tilde{\phi}_f \le 1$, which corresponds to $7/10 \le \tilde{\phi}_C \le 1$ altering the last portion of the profile to be given by $\tilde{\phi}_f = \tilde{\phi}_C/3 + 2/3$. Other modifications are also possible (e.g., one may decide to modify the horizontal portion of the composite profile in the $0.95 \le \tilde{\phi}_f \le 1$ region). A similar modification can also be made for the bounded CD scheme to improve its convergence characteristics. The modified NVDs of SMART, STOIC, and SUPERBEE schemes are shown in Fig. 12.7.

Mathematically, the functional relationships of the composite HR schemes displayed in Figs. 12.6 and 12.7 are given by

$$\text{MINMOD} \quad \tilde{\phi}_f = \begin{cases} \frac{3}{2}\tilde{\phi}_C & 0 \le \tilde{\phi}_C \le \frac{1}{2} \\ \frac{1}{2}\tilde{\phi}_C + \frac{1}{2} & \frac{1}{2} \le \tilde{\phi}_C \le 1 \\ \tilde{\phi}_C & \textit{elsewhere} \end{cases} \tag{12.14}$$

$$\text{Bounded CD} \quad \tilde{\phi}_f = \begin{cases} \frac{1}{2}\tilde{\phi}_C + \frac{1}{2} & 0 \le \tilde{\phi}_C \le 1 \\ \tilde{\phi}_C & \textit{elsewhere} \end{cases} \tag{12.15}$$

$$\text{OSHER} \quad \tilde{\phi}_f = \begin{cases} \frac{3}{2}\tilde{\phi}_C & 0 \le \tilde{\phi}_C \le \frac{2}{3} \\ 1 & \frac{2}{3} \le \tilde{\phi}_C \le 1 \\ \tilde{\phi}_C & \textit{elsewhere} \end{cases} \tag{12.16}$$

$$\text{SMART} \quad \tilde{\phi}_f = \begin{cases} \frac{3}{4}\tilde{\phi}_C + \frac{3}{8} & 0 \le \tilde{\phi}_C \le \frac{5}{6} \\ 1 & \frac{5}{6} \le \tilde{\phi}_C \le 1 \\ \tilde{\phi}_C & \textit{elsewhere} \end{cases} \tag{12.17}$$

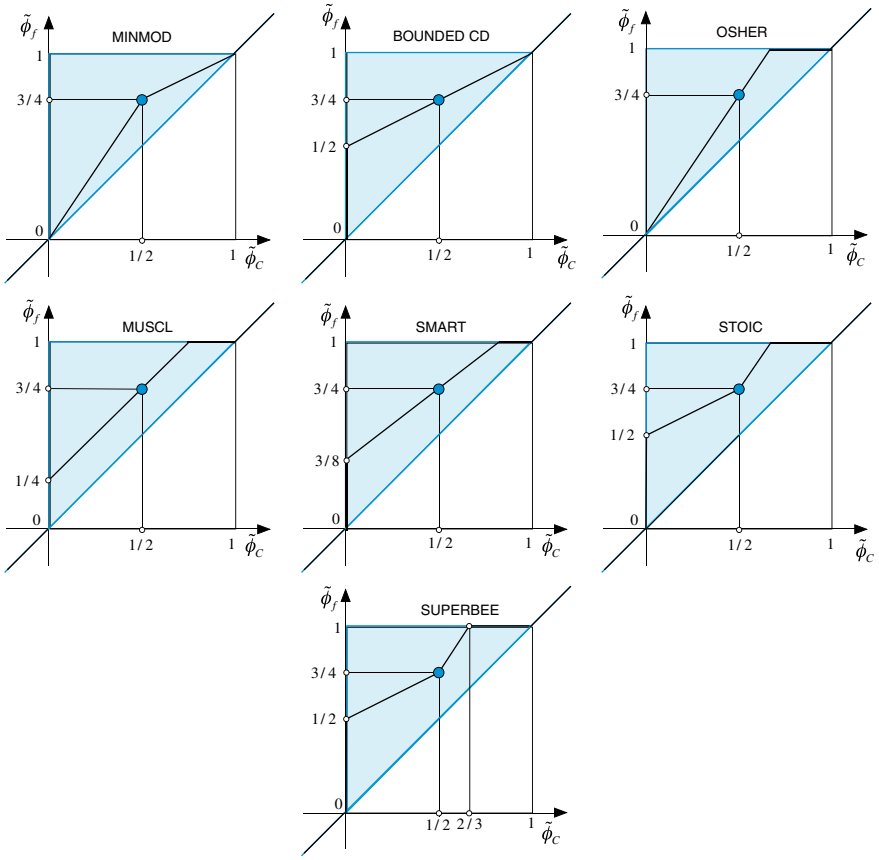

Fig. 12.6 NVD of several HR schemes

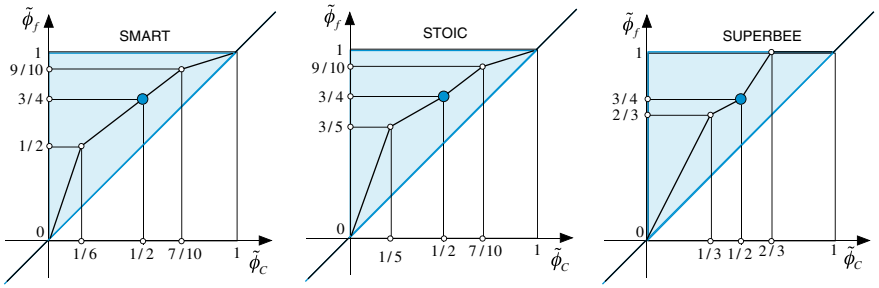

Fig. 12.7 NVD of the modified SMART, STOIC, and SUPERBEE schemes

$$\text{Modified SMART} \quad \tilde{\phi}_f = \begin{cases} 3\tilde{\phi}_C & 0 \le \tilde{\phi}_C \le \dfrac{1}{6} \\ \dfrac{3}{4}\tilde{\phi}_C + \dfrac{3}{8} & \dfrac{1}{6} \le \tilde{\phi}_C \le \dfrac{7}{10} \\ \dfrac{1}{3}\tilde{\phi}_C + \dfrac{2}{3} & \dfrac{7}{10} \le \tilde{\phi}_C \le 1 \\ \tilde{\phi}_C & \textit{elsewhere} \end{cases} \tag{12.18}$$

$$\text{STOIC} \quad \tilde{\phi}_f = \begin{cases} \dfrac{1}{2}\tilde{\phi}_C + \dfrac{1}{2} & 0 \le \tilde{\phi}_C \le \dfrac{1}{2} \\ \dfrac{3}{4}\tilde{\phi}_C + \dfrac{3}{8} & \dfrac{1}{2} \le \tilde{\phi}_C \le \dfrac{5}{6} \\ 1 & \dfrac{5}{6} \le \tilde{\phi}_C \le 1 \\ \tilde{\phi}_C & \textit{elsewhere} \end{cases} \tag{12.19}$$

$$\text{Modified STOIC} \quad \tilde{\phi}_f = \begin{cases} 3\tilde{\phi}_C & 0 \le \tilde{\phi}_C \le \dfrac{1}{5} \\ \dfrac{1}{2}\tilde{\phi}_C + \dfrac{1}{2} & \dfrac{1}{5} \le \tilde{\phi}_C \le \dfrac{1}{2} \\ \dfrac{3}{4}\tilde{\phi}_C + \dfrac{3}{8} & \dfrac{1}{2} \le \tilde{\phi}_C \le \dfrac{7}{10} \\ \dfrac{1}{3}\tilde{\phi}_C + \dfrac{2}{3} & \dfrac{7}{10} \le \tilde{\phi}_C \le 1 \\ \tilde{\phi}_C & \textit{elsewhere} \end{cases} \tag{12.20}$$

$$\text{MUSCL} \quad \tilde{\phi}_f = \begin{cases} 2\tilde{\phi}_C & 0 \le \tilde{\phi}_C \le \dfrac{1}{4} \\ \tilde{\phi}_C + \dfrac{1}{4} & \dfrac{1}{4} \le \tilde{\phi}_C \le \dfrac{3}{4} \\ 1 & \dfrac{3}{4} \le \tilde{\phi}_C \le 1 \\ \tilde{\phi}_C & \textit{elsewhere} \end{cases} \tag{12.21}$$

$$\text{SUPERBEE} \quad \tilde{\phi}_f = \begin{cases} \dfrac{1}{2} + \dfrac{1}{2}\tilde{\phi}_C & 0 \le \tilde{\phi}_C \le \dfrac{1}{2} \\ \dfrac{3}{2}\tilde{\phi}_C & \dfrac{1}{2} \le \tilde{\phi}_C \le \dfrac{2}{3} \\ 1 & \dfrac{2}{3} \le \tilde{\phi}_C \le 1 \\ \tilde{\phi}_C & \textit{elsewhere} \end{cases} \tag{12.22}$$

$$\text{Modified SUPERBEE} \quad \tilde{\phi}_f = \begin{cases} 2\tilde{\phi}_C & 0 \le \tilde{\phi}_C \le \frac{1}{3} \\ \frac{1}{2}\tilde{\phi}_C + \frac{1}{2} & \frac{1}{3} \le \tilde{\phi}_C \le \frac{1}{2} \\ \frac{3}{2}\tilde{\phi}_C & \frac{1}{2} \le \tilde{\phi}_C \le \frac{2}{3} \\ 1 & \frac{2}{3} \le \tilde{\phi}_C \le 1 \\ \tilde{\phi}_C & \textit{elsewhere} \end{cases} \tag{12.23}$$

Many other schemes were developed following this methodology such as CLAM [22], UTOPIA [23], SHARP [8], and ULTRA-SHARP [24, 25], to cite a few.

Example 3
Derive the NVF form of the SMART scheme.

Solution
Starting with the QUICK scheme, we have

$$\tilde{\phi}_{f,QUICK} = \frac{3}{4}\tilde{\phi}_C + \frac{3}{8}$$

On the NVF diagram this looks like the black line. In order to enforce the CBC, the interpolation profile of the QUICK scheme is modified to follow the blue lines as shown in the figure below

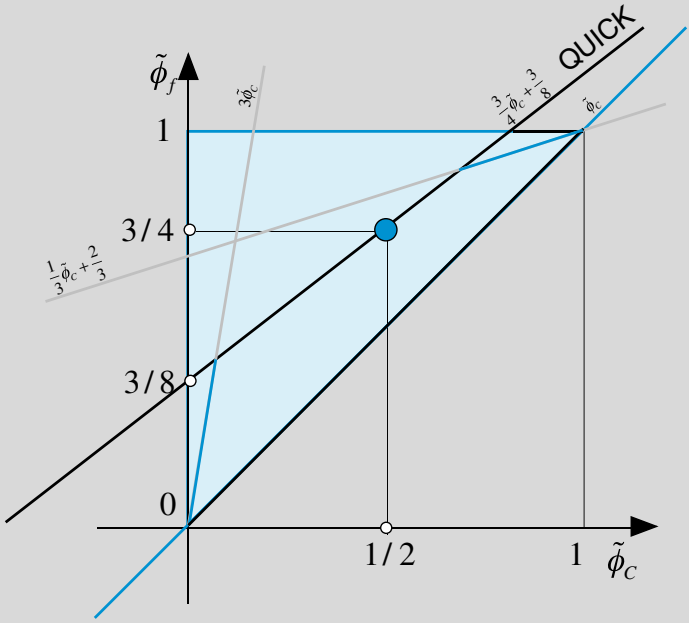

Thus the bounded QUICK scheme, now called the SMART scheme, is written as

$$\tilde{\phi}_f = \begin{cases} 3\tilde{\phi}_C & 0 \le \tilde{\phi}_C \le \dfrac{1}{6} \\ \dfrac{3}{4}\tilde{\phi}_C + \dfrac{3}{8} & \dfrac{1}{6} \le \tilde{\phi}_C \le \dfrac{7}{10} \\ \dfrac{1}{3}\tilde{\phi}_C + \dfrac{2}{3} & \dfrac{7}{10} \le \tilde{\phi}_C \le 1 \\ \tilde{\phi}_C & \textit{elsewhere} \end{cases}$$

12.4 The TVD Framework

Another popular approach for developing HR convective schemes is the Total Variation Diminishing (TVD) framework. In solving numerically an advection partial differential equation for a variable ϕ of the form presented so far, Total Variation (*TV*) is defined as

$$TV = \sum_i \left|\phi_{i+1} - \phi_i\right| \tag{12.24}$$

where i represents the index of a node in the spatial solution domain. A numerical method is said to be Total Variation Diminishing (TVD) if the *TV* in the solution does not increase with time. Mathematically this is equivalent to

$$TV\left(\phi^{t+\Delta t}\right) \le TV(\phi^t) \tag{12.25}$$

In his seminal paper, Harten [26] proved that a monotone scheme is TVD, and a TVD scheme is monotonicity preserving. A monotonicity preserving scheme does not create any new local extrema within the solution domain, i.e., the value of a local minimum is non-decreasing, and the value of a local maximum is non-increasing.

It is not intended here to give full mathematical derivations of the TVD approach. Rather, the intention is simply to explain the methodology for constructing TVD schemes. The approach used is based on the work of Sweby [27].

Consider the unsteady one-dimensional convection equation (11.73), which was used in the previous chapter to study the stability of convection schemes. In the absence of diffusion and sources this equation reduces to

$$\frac{\partial(\rho\phi)}{\partial t} = \underbrace{-\frac{\partial(\rho u\phi)}{\partial x}}_{RHS} \tag{12.26}$$

The general discretized form of the *RHS* term based on a five point stencil can be written as

$$RHS = -a(\phi_C - \phi_U) + b(\phi_D - \phi_C) \tag{12.27}$$

where U, C, and D represent the far upstream, upstream, and downstream nodes shown in Fig. 12.1a. Sweby and Harten proved that a sufficient condition for a numerical scheme presented by Eq. (12.27) to be TVD or monotone is for the coefficients per unit mass flow rate to satisfy the inequalities

$$a \geq 0, \; b \geq 0, \quad \text{and} \quad 0 \leq a + b \leq 1 \tag{12.28}$$

where the expressions for the coefficients a and b depend on the adopted convection scheme. Referring back to the convection schemes presented above, it was found that the first order upwind scheme is very diffusive while the second order central difference scheme is highly dispersive. The need is for a scheme that lies somewhere between the upwind and the central difference schemes, i.e., a scheme that has the stability of the upwind scheme and the accuracy of the central difference scheme. Such a scheme can be constructed starting from the central difference scheme written as

$$\phi_f = \underbrace{\frac{1}{2}(\phi_D + \phi_C)}_{CD} = \underbrace{\phi_C}_{upwind} + \underbrace{\frac{1}{2}(\phi_D - \phi_C)}_{anti-diffusive\,flux} \tag{12.29}$$

where the notation used earlier is adopted with C denoting the upwind node, D the downwind node, and f the value at the cell face straddling the C and D nodes. As implied by Eq. (12.29), the central difference scheme can be written as the sum of the upwind scheme and a flux which is supposed to be anti-diffusive since the CD scheme is dispersive. This flux is desirable as it makes the scheme second order accurate. The side effect is the unphysical oscillation it creates due to the decrease in numerical diffusion. Therefore a better approach would be one in which a portion of this anti-diffusive flux is added to the upwind scheme in such a way that the second order accuracy is preserved without creating any unphysical oscillations. One way to do that is to multiply this flux by a limiter function (also called limiter or flux limiter) that will prevent its excessive use in regions where oscillations might occur (e.g., across large gradients) while maximizing its contribution in smooth areas. Denoting such a limiter by $\psi(r)$, where r is usually taken as the ratio of two consecutive gradients, ϕ_f is calculated as

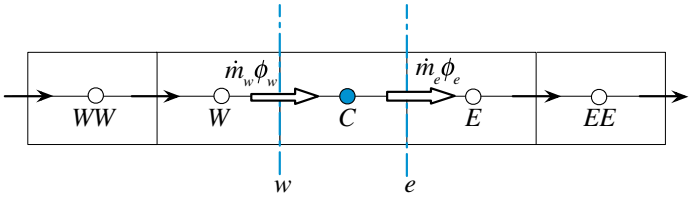

Fig. 12.8 Convective fluxes in a one dimensional domain

$$\phi_f = \phi_C + \frac{1}{2}\psi(r_f)(\phi_D - \phi_C) \text{ with } r_f = \frac{\phi_C - \phi_U}{\phi_D - \phi_C} \tag{12.30}$$

where U is the node upwind to C and D the node downwind to C. In order to preserve the sign of the anti-diffusive flux, $\psi(r_f)$ is taken to be nonnegative. Therefore developing a TVD scheme reduces to finding limiters that will make the numerical scheme TVD or monotone. The conditions that these limiters have to satisfy in order for the convection scheme to be monotonicity preserving are derived next by invoking the flux limiter in the discretization of the *RHS* of Eq. (12.27) via the interface values given by Eq. (12.30).

Considering the one dimensional domain shown in Fig. 12.8, the convective fluxes at the element faces are given by

$$\begin{aligned}
\dot{m}_e\phi_e &= \left[\phi_C + \frac{1}{2}\psi(r_e^+)(\phi_E - \phi_C)\right]\|\dot{m}_e, 0\| \\
&\quad - \left[\phi_E + \frac{1}{2}\psi(r_e^-)(\phi_C - \phi_E)\right]\|-\dot{m}_e, 0\| \\
\dot{m}_w\phi_w &= \left[\phi_C + \frac{1}{2}\psi(r_w^+)(\phi_W - \phi_C)\right]\|\dot{m}_w, 0\| \\
&\quad - \left[\phi_W + \frac{1}{2}\psi(r_w^-)(\phi_C - \phi_W)\right]\|-\dot{m}_w, 0\| \\
r_e^+ &= \frac{\phi_C - \phi_W}{\phi_E - \phi_C}, r_e^- = \frac{\phi_E - \phi_{EE}}{\phi_C - \phi_E}, \\
r_w^+ &= \frac{\phi_C - \phi_E}{\phi_W - \phi_C}, r_w^- = \frac{\phi_W - \phi_{WW}}{\phi_C - \phi_W}
\end{aligned} \tag{12.31}$$

To simplify the derivations to follow, a positive velocity is assumed. Under these conditions, the discretized form of the *RHS* of Eq. (12.24) is obtained as

$$RHS = -\dot{m}_e\left[\phi_C + \frac{1}{2}\psi(r_e^+)(\phi_E - \phi_C)\right] - \dot{m}_w\left[\phi_W + \frac{1}{2}\psi(r_w^-)(\phi_C - \phi_W)\right] \tag{12.32}$$

while the continuity equation is given by

$$\dot{m}_e + \dot{m}_w = 0 \Rightarrow \dot{m}_w = -\dot{m}_e \tag{12.33}$$

Invoking the continuity constraint, the *RHS* equation can be rearranged into

$$\begin{aligned}
RHS &= -\dot{m}_e\left[1 + \frac{1}{2}\psi(r_e^+)\underbrace{\frac{(\phi_E - \phi_C)}{(\phi_C - \phi_W)}}_{1/r_e^+} - \frac{1}{2}\psi(r_w^-)\right](\phi_C - \phi_W) \\
&= -\dot{m}_e\left[1 + \frac{1}{2}\frac{\psi(r_e^+)}{r_e^+} - \frac{1}{2}\psi(r_w^-)\right](\phi_C - \phi_W)
\end{aligned} \tag{12.34}$$

Comparing Eq. (12.34) with Eq. (12.27), the values of a and b are found to be

$$a = 1 + \frac{1}{2}\frac{\psi(r_e^+)}{r_e^+} - \frac{1}{2}\psi(r_w^-) \quad b = 0 \tag{12.35}$$

For the scheme to be TVD, the following should hold [Eq. (12.28)]:

$$0 \le 1 + \frac{1}{2}\frac{\psi(r_e^+)}{r_e^+} - \frac{1}{2}\psi(r_w^-) \le 1 \tag{12.36}$$

which can be expanded to

$$\begin{aligned} 1 + \frac{1}{2}\frac{\psi(r)}{r} - \frac{1}{2}\psi(r) \ge 0 &\Rightarrow \frac{1}{2}\frac{\psi(r)}{r} - \frac{1}{2}\psi(r) \ge -1 \Rightarrow \psi(r) - \frac{\psi(r)}{r} \le 2 \\ 1 + \frac{1}{2}\frac{\psi(r)}{r} - \frac{1}{2}\psi(r) \le 1 &\Rightarrow \frac{1}{2}\frac{\psi(r)}{r} - \frac{1}{2}\psi(r) \le 0 \Rightarrow \psi(r) - \frac{\psi(r)}{r} \ge 0 \end{aligned} \tag{12.37}$$

or simply

$$0 \le \psi(r) - \frac{\psi(r)}{r} \le 2 \tag{12.38}$$

If in addition to having $\psi(r) \ge 0$, a condition is imposed whereby $\psi(r) = 0$ for negative values of r, then the above conditions will be satisfied if

$$\psi(r) \le 2 \quad \text{and} \quad \psi(r) \le 2r \tag{12.39}$$

Combining all conditions that the limiter has to satisfy to produce a TVD scheme, a criterion similar to the CBC can be developed and is given by

$$\psi(r) = \begin{cases} \min(2r, 2) & r > 0 \\ 0 & r \le 0 \end{cases} \tag{12.40}$$

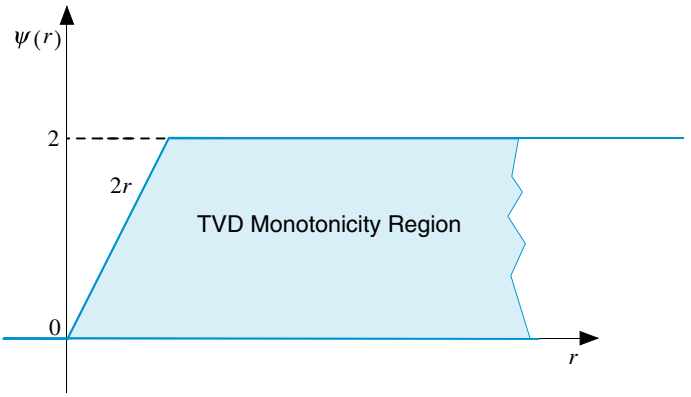

Fig. 12.9 TVD monotonicity region on a $r - \psi$ diagram

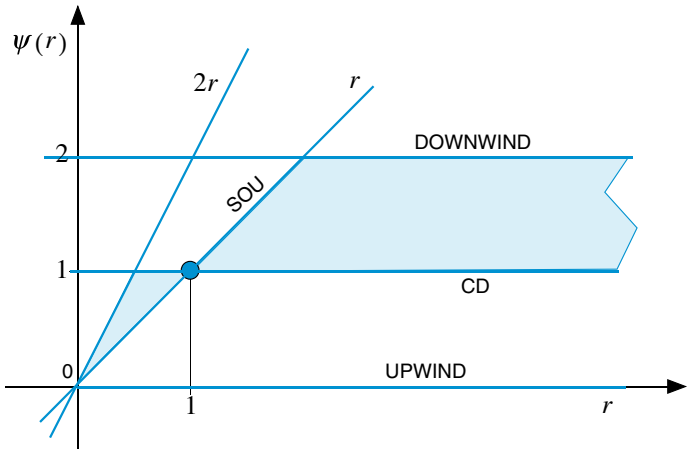

Fig. 12.10 Limiters of SOU and CD schemes on a $r - \psi$ diagram

As depicted in Fig. 12.9, these conditions can be drawn on a $r - \psi$ diagram, which is also denoted by Sweby's diagram, to show the TVD monotonicity region (blue region in the plot). Using this diagram, it is simple to grasp the formulation of TVD schemes. Any flux limiter $\psi(r)$ formulated to lie within the TVD monotonicity region yields a TVD scheme. Sweby's diagram is very similar to the NVD presented above.

The limiters for all schemes presented so far can be derived and their functional relationships drawn on Sweby's diagram. In specific the limiter of the CD is easily obtained from Eq. (12.29) as $\psi^{CD}(r_f) = 1$ while that of the SOU scheme can be computed as follows:

$$\begin{aligned} \phi_f &= \phi_C + \frac{1}{2}\psi^{SOU}(r_f)(\phi_D - \phi_C) = \frac{3}{2}\phi_C - \frac{1}{2}\phi_U \\ \Rightarrow \psi^{SOU}(r_f) &= \frac{\phi_C - \phi_U}{\phi_D - \phi_C} = r_f \end{aligned} \tag{12.41}$$

The limiters for both schemes are displayed in Fig. 12.10.

Sweby [27] also noted that because $\psi(r_f) = 0$ for $r_f < 0$, second order accuracy is lost at extrema of the solution. The SOU and CD schemes are second order schemes and by inspecting Fig. 12.10 it is clearly seen that both of them pass through the point (1, 1). In addition, as demonstrated in the work of Van Leer [28], any second order scheme can be written as a weighted average of the CD and SOU schemes. Thus for a scheme to be second order its limiter has to pass through the point (1, 1) and, as shown in Fig. 12.10, its limiter should lie in the region bordered by the CD and SOU limiters (blue region in the plot). The corresponding region on an NVD is shown in Fig. 12.11.

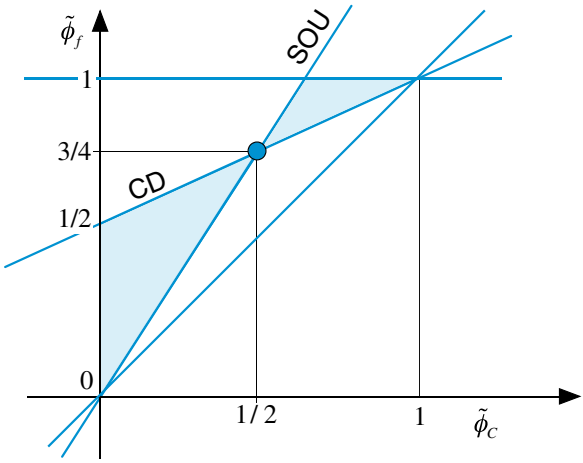

Fig. 12.11 Region on an NVD equivalent to the TVD monotonicity region on a Sweby's diagram for second order schemes

Adopting this approach and following the procedure used with the SOU scheme, the functional relationships of the limiters for many of the HO schemes presented above can be easily computed and are given by

$$\begin{cases} \textit{Upwind} & \psi(r_f) = 0 \\ \textit{Downwind} & \psi(r_f) = 2 \\ \textit{FROMM} & \psi(r_f) = \dfrac{1+r_f}{2} \\ \textit{SOU} & \psi(r_f) = r_f \\ \textit{CD} & \psi(r_f) = 1 \\ \textit{QUICK} & \psi(r_f) = \dfrac{3+r_f}{4} \end{cases} \tag{12.42}$$

The FROMM scheme is the average of the CD and SOU scheme. Its functional relationship is mathematically written as

$$\left.\begin{aligned} \phi_f &= \frac{1}{2}\left(\frac{\phi_C+\phi_D}{2}+\frac{3}{2}\phi_C-\frac{1}{2}\phi_U\right) = \phi_C+\frac{\phi_D-\phi_U}{4} \\ \phi_f &= \phi_C+\frac{1}{2}\psi(r_f)(\phi_D-\phi_C) \end{aligned}\right\} \Rightarrow \psi(r_f) = \frac{1+r_f}{2} \tag{12.43}$$

The functional relationships of these limiters are displayed in Fig. 12.12. With the exception of the upwind scheme limiter all others are seen not to be totally lying within the monotonicity region. As such these schemes are unbounded.

By limiting the $\psi(r_f)$ functions of the various schemes given above to lie within the monotonicity region displayed in Fig. 12.9, these HO schemes are transformed into HR TVD schemes. Many TVD schemes have been developed in that manner and the limiters for a number of them are shown in Fig. 12.13a–d with the functional relationships of their limiters given by

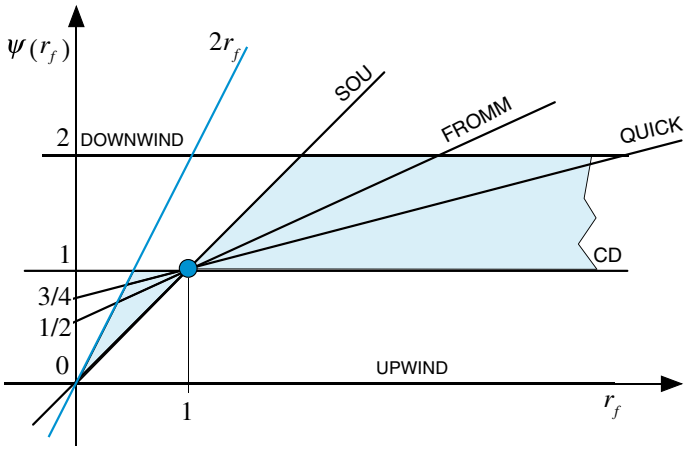

Fig. 12.12 High Order schemes and TVD monotonicity region on Sweby's diagram

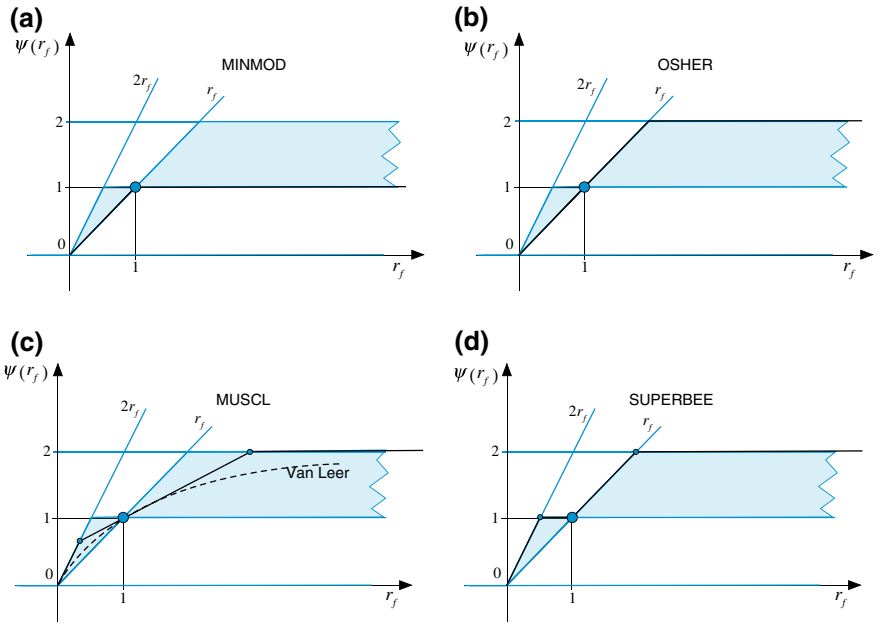

Fig. 12.13 Limiters of the **a** MINMOD, **b** OSHER, **c** MUSCL, and **d** SUPERBEE TVD schemes on a Sweby diagram

$$\begin{cases} SUPERBEE & \psi(r_f) = \max\left(0, \min\left(1, 2r_f\right), \min\left(2, r_f\right)\right) \\ MINMOD & \psi(r_f) = \max\left(0, \min\left(1, r_f\right)\right) \\ OSHER & \psi(r_f) = \max\left(0, \min\left(2, r_f\right)\right) \\ Van\ Leer & \psi(r_f) = \dfrac{r_f + |r_f|}{1 + |r_f|} \\ MUSCL & \psi(r_f) = \max\left(0, \min\left(2r_f, \left(r_f + 1\right)/2, 2\right)\right) \end{cases} \tag{12.44}$$

12.5 The NVF-TVD Relation

Both NVF and TVD formulations enforce Boundedness following different approaches, which can be demonstrated to be somewhat related. This is done by first deriving a relation between r_f and $\tilde{\phi}_C$, then comparing the NVF-CBC (Eq. 12.13) with the TVD-CBC (Eq. 12.40), and finally presenting the general transformation that allows the functional relationship of any TVD scheme to be written in the NVF framework and vice versa.

The relation between r_f and $\tilde{\phi}_C$ can be easily derived starting with the definition of r_f and is obtained as

$$\begin{aligned} r_f &= \frac{\phi_C - \phi_U}{\phi_D - \phi_C} = \frac{(\phi_C - \phi_U)/(\phi_D - \phi_U)}{(\phi_D - \phi_U + \phi_U - \phi_C)/(\phi_D - \phi_U)} \\ &= \frac{\tilde{\phi}_C}{1 - \tilde{\phi}_C} \Rightarrow \tilde{\phi}_C = \frac{r_f}{1 + r_f} \end{aligned} \tag{12.45}$$

Using Eq. (12.45) a number of linear schemes can be compared in the two frameworks. The limiter $\psi(r_f) = 0$, which represents the Upwind scheme in the TVD formulation is also equivalent to the upwind scheme in the NVF formulation (i.e., $\tilde{\phi}_f = \tilde{\phi}_C$). This follows from the fact that $\psi(r_f) = 0 \Rightarrow \phi_f = \phi_U \Rightarrow \tilde{\phi}_f = \tilde{\phi}_C$. The upwind scheme is imposed as a limit for the TVD-CBC when $r_f \leq 0$, the equivalent condition in the NVF-CBC is obtained as

$$r_f \leq 0 \Rightarrow \frac{\tilde{\phi}_C}{1 - \tilde{\phi}_C} \leq 0 \Rightarrow \begin{cases} \tilde{\phi}_C \leq 0 \\ \tilde{\phi}_C > 1 \end{cases} \tag{12.46}$$

These also represent the conditions for imposing the Upwind scheme in the NVF-CBC.

Moreover, on the NVF-CBC, the functional relationship has to increase monotonically in the region $0 \leq \tilde{\phi}_C \leq 1$. On Sweby's diagram the region extends over the interval $0 \leq r_f < +\infty$. Both regions represent the same interval as demonstrated by the following relation:

$$\tilde{\phi}_C \to 1 \Rightarrow r_f = \frac{\tilde{\phi}_C}{1-\tilde{\phi}_C} \to +\infty \tag{12.47}$$

Further, for the TVD-CBC condition

$$\psi(r_f) \leq 2 \tag{12.48}$$

the equivalent condition in the NVF-CBC can be obtained as follows:

$$\left.\begin{aligned} &\psi(r_f) = 2 \\ &\phi_f = \phi_C + \frac{1}{2}\psi(r_f)(\phi_D - \phi_C) \end{aligned}\right\} \Rightarrow \phi_f = \phi_C + (\phi_D - \phi_C) = \phi_D \Rightarrow \tilde{\phi}_f = 1 \tag{12.49}$$

Thus,

$$\psi(r_f) \leq 2 \Rightarrow \tilde{\phi}_f \leq 1 \tag{12.50}$$

which is the condition that should be satisfied by the NVF-CBC. The last condition imposed by the TVD-CBC on $\psi(r_f)$ is given by

$$\psi(r_f) \leq 2r_f \tag{12.51}$$

The equivalent condition using the NVF-CBC is obtained as

$$\left.\begin{aligned} &\psi(r_f) = 2r_f \\ &\phi_f = \phi_C + \frac{1}{2}\psi(r_f)(\phi_D - \phi_C) \end{aligned}\right\} \Rightarrow \phi_f = \phi_C + \frac{\phi_C - \phi_U}{\phi_D - \phi_C}(\phi_D - \phi_C) = 2\phi_C - \phi_U \tag{12.52}$$

which can be normalized to yield

$$\phi_f = 2\phi_C - \phi_U \Rightarrow \phi_f - \phi_U = 2\phi_C - 2\phi_U \Rightarrow \tilde{\phi}_f = 2\tilde{\phi}_C \tag{12.53}$$

This is more restrictive than the NVF-CBC and is the only difference between the two formulations. Based on this condition, the TVD-CBC and the modified NVF-CBC would look as shown in Fig. 12.14a with the monotonicity region reduced to the upwind line and the blue area. While the modified TVD-CBC and the NVF-CBC (i.e., the condition $\tilde{\phi}_C = 0$ on the NVF-CBC corresponds to $r_f = 0$ on the TVD-CBC) would look as shown in Fig. 12.14b. Regarding second order accuracy, it was stated that for a TVD scheme to be second order accurate it has to pass through the point (1, 1), i.e., $\psi(1) = 1$. The equivalent values using the NVF are found as

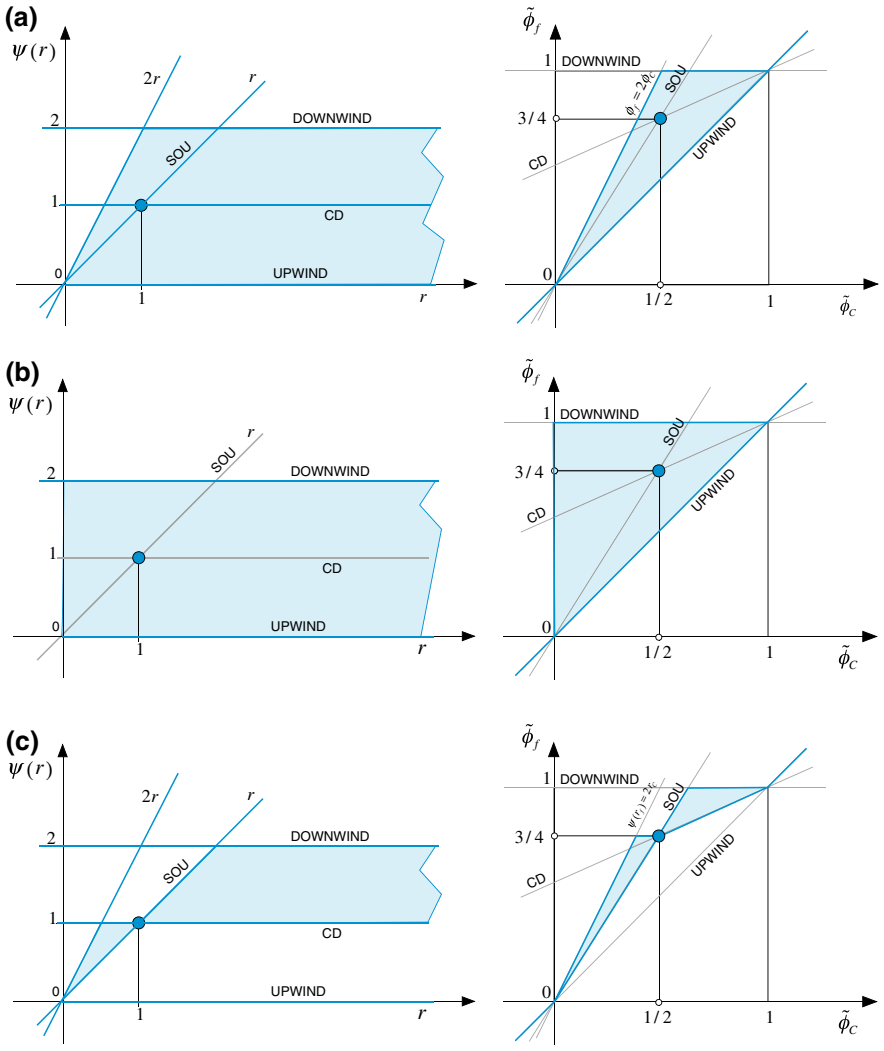

Fig. 12.14 **a** TVD-CBC on Sweby and Normalized Variable Diagrams. **b** NVF-CBC on Sweby and Normalized Variable Diagrams. **c** TVD-CBC on Sweby and Normalized Variable Diagrams for second order schemes

$$
\begin{aligned}
r_f = 1 \Rightarrow \frac{\tilde{\phi}_C}{1-\tilde{\phi}_C} = 1 \Rightarrow \tilde{\phi}_C = 1 - \tilde{\phi}_C \Rightarrow \tilde{\phi}_C = 0.5 \\
\phi_f = \phi_C + \frac{1}{2}\psi(1)(\phi_D - \phi_C) = \phi_C + \frac{1}{2}(\phi_D - \phi_C) = \frac{1}{2}(\phi_D + \phi_C) \\
\therefore \phi_f - \phi_U = \frac{1}{2}(\phi_D - \phi_U + \phi_C - \phi_U) \Rightarrow \tilde{\phi}_f = \frac{1}{2}\left(1 + \tilde{\phi}_C\right) = 0.75
\end{aligned}
\tag{12.54}
$$

which is exactly the point $Q(0.5, 0.75)$ found in the NFV. As stated earlier, Van Leer demonstrated that any second order scheme can be written as a weighted average of the CD and SOU schemes. Therefore its functional relationship should lie between the functional relationships of the CD and SOU schemes with their TVD-CBC monotonicity regions reduced to the upwind line and the blue area shown on a Sweby diagram and an NVD in Fig. 12.14c.

The above procedure can be generalized to transform any TVD scheme into an equivalent NVF scheme and vice versa. Starting with a scheme in the NVF framework, the value at the face ϕ_f is expressed as

$$\phi_f = f\left(\tilde{\phi}_C\right)(\phi_D - \phi_U) + \phi_U \text{ with } \tilde{\phi}_C = \frac{\phi_C - \phi_U}{\phi_D - \phi_U} \tag{12.55}$$

whereas for a TVD scheme ϕ_f is given by

$$\phi_f = \phi_C + \frac{1}{2}\psi(r_f)(\phi_D - \phi_C) \text{ with } r_f = \frac{\phi_C - \phi_U}{\phi_D - \phi_C} \tag{12.56}$$

Equating the above two ϕ_f equations, yields

$$\phi_f = \phi_C + \frac{1}{2}\psi(r_f)(\phi_D - \phi_C) = f\left(\tilde{\phi}_C\right)(\phi_D - \phi_U) + \phi_U \tag{12.57}$$

Thus

$$\psi(r_f)\frac{(\phi_D - \phi_C)}{(\phi_D - \phi_U)} = 2\frac{f\left(\tilde{\phi}_C\right)(\phi_D - \phi_U)}{(\phi_D - \phi_U)} - 2\frac{(\phi_C - \phi_U)}{(\phi_D - \phi_U)} = 2\left(f\left(\tilde{\phi}_C\right) - \tilde{\phi}_C\right) \tag{12.58}$$

The term on the left hand side of the above equation can be modified to

$$\psi(r_f)\frac{(\phi_D - \phi_C)}{(\phi_D - \phi_U)} = \psi(r_f)\frac{(\phi_D - \phi_U - \phi_C + \phi_U)}{(\phi_D - \phi_U)} = \psi(r_f)\left(1 - \tilde{\phi}_C\right) \tag{12.59}$$

leading to

$$\psi(r_f)\left(1 - \tilde{\phi}_C\right) = 2\frac{f\left(\tilde{\phi}_C\right)(\phi_D - \phi_U) - (\phi_C - \phi_U)}{(\phi_D - \phi_U)} = \psi(r_f) = 2\frac{f\left(\tilde{\phi}_C\right) - \tilde{\phi}_C}{1 - \tilde{\phi}_C} \tag{12.60}$$

Equation (12.60) may also be written as

$$f\left(\tilde{\phi}_C\right) = \frac{\psi(r_f) + 2r_f}{2(1 + r_f)} \tag{12.61}$$

As an example, the functional relationship of the UPWIND Scheme in the NVF framework is $\tilde{\phi}_f = \tilde{\phi}_C$, its TVD limiter is found as

$$\tilde{\phi}_f = \tilde{\phi}_C \Rightarrow \psi(r_f) = 2\frac{f\left(\tilde{\phi}_C\right) - \tilde{\phi}_C}{1 - \tilde{\phi}_C} = 2\frac{\tilde{\phi}_C - \tilde{\phi}_C}{1 - \tilde{\phi}_C} = 0 \tag{12.62}$$

The TVD limiter for the DOWNWIND Scheme is $\psi(r_f) = 2$, its NVF functional relationship can be obtained as

$$\tilde{\phi}_f = f\left(\tilde{\phi}_C\right) = \frac{\psi(r_f) + 2r_f}{2(1 + r_f)} = \frac{2 + 2r_f}{2(1 + r_f)} = 1 \tag{12.63}$$

Knowing the NVF form of the SOU scheme, its TVD limiter is computed as

$$\tilde{\phi}_f = \frac{3}{2}\tilde{\phi}_C \Rightarrow \psi(r_f) = 2\frac{\left(\frac{3}{2}\tilde{\phi}_C - \tilde{\phi}_C\right)}{\left(1 - \tilde{\phi}_C\right)} = 2\frac{\left(0.5\tilde{\phi}_C\right)}{\left(1 - \tilde{\phi}_C\right)} = \frac{\tilde{\phi}_C}{\left(1 - \tilde{\phi}_C\right)} = r_f \tag{12.64}$$

The same is applicable to other schemes.

Example 4
Starting with the TVD-Van Leer formulation, derive the NVF-Van Leer scheme.

Solution
The TVD-Van Leer limiter is given by

$$\psi(r_f) = \frac{r_f + |r_f|}{1 + |r_f|}.$$

Noting that

$$r_f = \frac{\tilde{\phi}_C}{1 - \tilde{\phi}_C}$$

its TVD functional relationship is transformed to

$$\psi(r_f) = \frac{\frac{\tilde{\phi}_C}{1 - \tilde{\phi}_C} + \left|\frac{\tilde{\phi}_C}{1 - \tilde{\phi}_C}\right|}{1 + \left|\frac{\tilde{\phi}_C}{1 - \tilde{\phi}_C}\right|} = \frac{\frac{|1 - \tilde{\phi}_C|}{1 - \tilde{\phi}_C}\tilde{\phi}_C + |\tilde{\phi}_C|}{|1 - \tilde{\phi}_C| + |\tilde{\phi}_C|}$$

Combining the above equation with the TVD relationship in normalized form, which is given by,

$$\tilde{\phi}_f = \tilde{\phi}_C + \frac{1}{2}\psi(r_f)\left(1 - \tilde{\phi}_C\right)$$

yields

$$\begin{aligned}\tilde{\phi}_f &= \tilde{\phi}_C + \frac{1}{2}\psi(r_f)\left(1 - \tilde{\phi}_C\right) \\ &= \tilde{\phi}_C + \frac{1}{2}\frac{\frac{\left|1-\tilde{\phi}_C\right|}{1-\tilde{\phi}_C}\tilde{\phi}_C + \left|\tilde{\phi}_C\right|}{\left|1-\tilde{\phi}_C\right| + \left|\tilde{\phi}_C\right|}\left(1 - \tilde{\phi}_C\right)\end{aligned}$$

The following three cases are identified:

a. Case 1: $0 < \tilde{\phi}_C < 1$
In this case $\left|\tilde{\phi}_C\right| = \tilde{\phi}_C$ and $\left|1 - \tilde{\phi}_C\right| = 1 - \tilde{\phi}_C$, thus

$$\left.\begin{aligned}&\psi(r_f) = 2\tilde{\phi}_C \\ &\tilde{\phi}_f = \tilde{\phi}_C + \frac{1}{2}\psi(r_f)\left(1 - \tilde{\phi}_C\right)\end{aligned}\right\} \tilde{\phi}_f = \tilde{\phi}_C + \tilde{\phi}_C\left(1 - \tilde{\phi}_C\right) = 2\tilde{\phi}_C - \left(\tilde{\phi}_C\right)^2$$

b. Case 2: $\tilde{\phi}_C > 1$
In this case $\left|\tilde{\phi}_C\right| = \tilde{\phi}_C$ and $\left|1 - \tilde{\phi}_C\right| = \tilde{\phi}_C - 1$, thus

$$\left.\begin{aligned}&\psi(r_f) = 0 \\ &\tilde{\phi}_f = \tilde{\phi}_C + \frac{1}{2}\psi(r_f)\left(1 - \tilde{\phi}_C\right)\end{aligned}\right\} \tilde{\phi}_f = \tilde{\phi}_C$$

c. Case 3: $\tilde{\phi}_C < 0$
In this case $\left|\tilde{\phi}_C\right| = -\tilde{\phi}_C$ and $\left|1 - \tilde{\phi}_C\right| = 1 - \tilde{\phi}_C$, thus

$$\left.\begin{aligned}&\psi(r_f) = 0 \\ &\tilde{\phi}_f = \tilde{\phi}_C + \frac{1}{2}\psi(r_f)\left(1 - \tilde{\phi}_C\right)\end{aligned}\right\} \tilde{\phi}_f = \tilde{\phi}_C$$

Combining the results of the three cases into one NVF formulation, the functional relationship of the Van Leer Scheme becomes

$$\tilde{\phi}_{f,\text{VanLeer}} = \begin{cases} 2\tilde{\phi}_C - \left(\tilde{\phi}_C\right)^2 & 0 < \tilde{\phi}_C < 1 \\ \tilde{\phi}_C & \textit{otherwise} \end{cases}$$

12.6 HR Schemes in Unstructured Grid Systems

As mentioned in Chap. 11, another alternative that can be followed to overcome the hurdle of not having a clear upwind location U in unstructured grids, which is needed in the calculation of $\tilde{\phi}_C$ or r_f, is to create a virtual one. As depicted in Fig. 12.15, the easiest way is to assume U to lie on the line joining the nodes C and D such that C is the midpoint of the segment joining the points U and D. With this assumption and based on the analysis done earlier, the following can be written:

$$\phi_D - \phi_U = \nabla\phi_C \cdot \mathbf{d}_{UD} = 2\nabla\phi_C \cdot \mathbf{d}_{CD} \tag{12.65}$$

from which the value of ϕ_U is computed as

$$\phi_U = \phi_D - 2\nabla\phi_C \cdot \mathbf{d}_{CD} \tag{12.66}$$

where $\mathbf{d}_{CD}$ is the vector between the nodes C and D, and $\mathbf{d}_{UD}$ is the vector between nodes D and the *virtual* node U. As mentioned above U is constructed such that C is taken to be the centre of the UD segment. With the value of ϕ_U computed, the use of either the NVF or the TVD approach proceeds as described above.

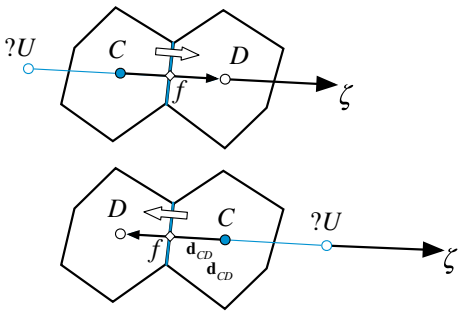

Fig. 12.15 Virtual upwind node in unstructured grids

12.7 Deferred Correction for HR Schemes

The numerical implementation of HR schemes is best understood through an example. For that purpose the multi dimensional advection equation with a source is considered. Again the velocity field is assumed to be known and the conservation equation in vector form is given by

$$\nabla \cdot (\rho \mathbf{v}\phi) = Q^{\phi} \tag{12.67}$$

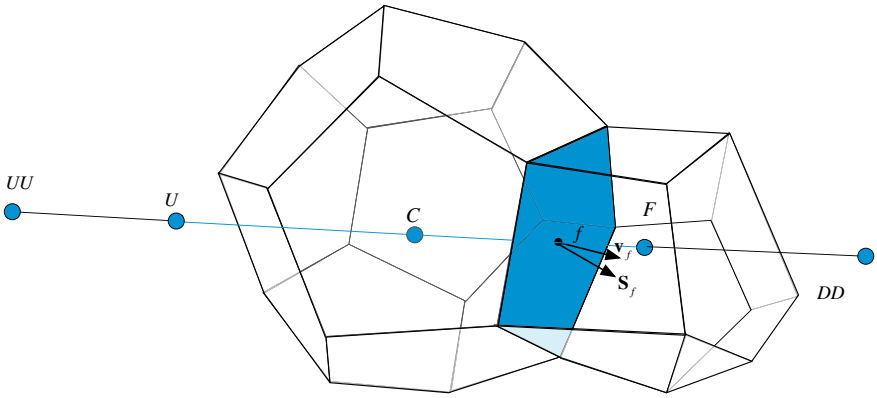

Fig. 12.16 Two three-dimensional elements, which represent part of an unstructured grid system

Integrating over the element of volume V_C shown in Fig. 12.16, applying the divergence theorem, and replacing the surface integral by a summation over the element faces, Eq. (12.67) becomes

$$\sum_{f\sim nb(C)} (\rho \mathbf{v}\phi)_f \cdot \mathbf{S}_f = Q_C^{\phi} V_C \tag{12.68}$$

Noticing that the mass flow rate at a cell face is given by

$$\dot{m}_f = (\rho \mathbf{v})_f \cdot \mathbf{S}_f \tag{12.69}$$

then Eq. (12.68) can be rewritten as

$$\sum_{f\sim nb(C)} \dot{m}_f \phi_f = Q_C^{\phi} \mathrm{V}_C \tag{12.70}$$

The value of ϕ_f is obtained using any of the advection schemes presented earlier keeping in mind that, in order to be able to solve for the unknown values at the main nodes, the algebraic form of the discretized equation should look like

$$a_C \phi_C + \sum_{F\sim NB(C)} a_F \phi_F = b_C \tag{12.71}$$

The difficulty lies in the instability that arises when expressing ϕ_f in terms of nodal values as described next.

12.7.1 The Difficulty with the Direct Use of Nodal Values

The difficulty that arises when explicitly expressing ϕ_f in terms of neighboring values will be explained by discretizing the convection flux using a TVD scheme. Referring to Fig. 12.16, the convective flux at a face f is written as

$$\begin{aligned}\dot{m}_f\phi_f = &\left[\phi_C + \frac{1}{2}\psi\overbrace{\left(\frac{\phi_C-\phi_U}{\phi_F-\phi_C}\right)}^{r_f^+}(\phi_F-\phi_C)\right]\|\dot{m}_f,0\| \\ &-\left[\phi_F + \frac{1}{2}\psi\overbrace{\left(\frac{\phi_F-\phi_{DD}}{\phi_C-\phi_F}\right)}^{r_f^-}(\phi_C-\phi_F)\right]\|-\dot{m}_f,0\| \\ &= \left[\phi_C + \frac{1}{2}\psi\left(r_f^+\right)(\phi_F-\phi_C)\right]\|\dot{m}_f,0\| \\ &\quad -\left[\phi_F + \frac{1}{2}\psi\left(r_f^-\right)(\phi_C-\phi_F)\right]\|-\dot{m}_f,0\|\end{aligned} \tag{12.72}$$

Substituting Eq. (12.72) into Eq. (12.70) yields

$$a_C\phi_C + \sum_{F\sim NB(C)} a_F\phi_F = b_C \tag{12.73}$$

where

$$\begin{aligned}a_F &= FluxF_f = -\|-\dot{m}_f,0\| + \frac{1}{2}\psi\left(r_f^+\right)\|\dot{m}_f,0\| + \frac{1}{2}\psi\left(r_f^-\right)\|-\dot{m}_f,0\| \\ a_C &= \sum_{f\sim nb(C)} FluxC_f = -\sum_{F\sim NB(C)} a_F + \sum_{F\sim NB(C)} \dot{m}_f \\ b_C &= Q_C^\phi V_C\end{aligned} \tag{12.74}$$

To see the weakness in this formulation, Eq. (12.67) is simplified to the one dimensional problem depicted in Fig. 12.8. Assuming the flow to be in the positive direction and using the terminology displayed in the figure, Eq. (12.73) becomes

$$a_C\phi_C + a_E\phi_E + a_W\phi_W = b_C \tag{12.75}$$

where

$$\begin{aligned} a_E &= FluxF_e = \frac{1}{2}\psi\left(r_e^+\right)\dot{m}_e \\ a_W &= FluxF_w = \left[-1+\frac{1}{2}\psi\left(r_w^-\right)\right]\dot{m}_e \\ a_C &= \sum_{f\sim nb(C)} FluxC_f = -(a_E + a_W) \\ b_C &= Q_C^{\phi} V_C \end{aligned} \tag{12.76}$$

Since $0 \le \psi(r) \le 2$, the a_E and a_W coefficients will be of opposite signs (except for the UPWIND scheme, i.e., when $\psi\left(r_f\right) = 0$), thereby violating one of the basic rules for stability and causing convergence difficulties of the iterative procedure. Following a similar approach with the NVF leads to the same shortcomings.

A remedy, which was presented in the previous chapter, is the deferred correction (DC) procedure, in which the coefficients are based on the upwind scheme, while the difference between the HR and upwind schemes is added as a source term in the algebraic equation. The DC procedure is simple to implement and can be used in structured and unstructured grid systems, however as the difference between the cell face values calculated with the upwind scheme and that calculated with the HR scheme becomes larger, the convergence rate diminishes. This effect can be easily estimated on an NVD; the difference between the UPWIND line and that of the chosen HR scheme is the normalized difference between the cell face values. The larger this difference is, the lower the convergence rate will be. This has enticed researchers to look for other techniques for implementing HR schemes that are more implicit not affecting the convergence rate. Two of these techniques are described in the next section.

12.8 The DWF and NWF Methods

Several techniques have been developed to overcome the reduction in the convergence rate associated with the use of the Deferred Correction (DC) procedure for the implementation of HR schemes. Two of these methods are presented below, namely the Downwind Weighing Factor (DWF) method of Leonard and Mokhtari [25] (implemented in OpenFOAM®) and the Normalized Weighing Factor (NWF) method of Darwish and Moukalled [29].

The implementation details for both methods are presented in the context of solving the convection equation (Eq. 12.67) over the three-dimensional unstructured grid system shown in Fig. 12.16. The discretized equation for the element of volume V_C shown in Fig. 12.16 can be written as

$$\sum_{f\sim nb(C)} \dot{m}_f \phi_f = Q_C^{\phi} V_C \tag{12.77}$$

The ϕ values at cell faces are computed using a HR scheme and the objective of the various methods is to incorporate these values in the discretized equation in the most effective manner.

12.8.1 The Downwind Weighing Factor (DWF) Method

The Downwind Weighing Factor (*DWF*) [25] defined as

$$DWF_f = \frac{\phi_f - \phi_C}{\phi_D - \phi_C} = \frac{\tilde{\phi}_f - \tilde{\phi}_C}{1 - \tilde{\phi}_C} \tag{12.78}$$

is used to rewrite the face value such that

$$\phi_f = DWF_f \phi_D + \left(1 - DWF_f\right)\phi_C = \phi_C + DWF_f(\phi_D - \phi_C) \tag{12.79}$$

thereby redistributing the HR scheme estimate ϕ_f or the normalized value $\tilde{\phi}_f$ between the Upwind and Downwind nodes. The effect is a reduced stencil for the discretized coefficients. Since the value of ϕ_f computed using a HR scheme lies between ϕ_C and ϕ_D, the value of DWF_f is always between 0 and 1, i.e., $0 \leq DWF_f \leq 1$.

Now rather than computing the DWF_f explicitly from the computed ϕ_f value, the DWF_f can be expressed directly from the functional relationships of the HR scheme. Table 12.1 presents such relationships for several HO and HR schemes on uniform grid.

Comparing the TVD formulation given by Eq. (12.30) with Eq. (12.79), it is clear that

$$DWF_f = \frac{1}{2}\psi(r_f) \tag{12.80}$$

As shown in the previous section on TVD schemes, the coefficients obtained from such implementation will not be diagonally dominant and the formulation is thus not stable for many flow configurations. As the method is used in OpenFOAM®, the reasons behind the numerical difficulties that are generally experienced by the code when solving convection dominated flow problems are now clear.

For completeness, the analysis of the implementation via the DWF is presented. Starting with Eq. (12.79), the convection flux in the general case is written in the form

$$\begin{aligned} \dot{m}_f \phi_f = {} & \left\|\dot{m}_f, 0\right\| \left[DWF_f^+ \phi_F + \left(1 - DWF_f^+\right)\phi_C\right] \\ & - \left\|-\dot{m}_f, 0\right\| \left[DWF_f^- \phi_C + \left(1 - DWF_f^-\right)\phi_F\right] \end{aligned} \tag{12.81}$$

with

$$\begin{aligned} DWF_f^+ &= \frac{\phi_f - \phi_C}{\phi_F - \phi_C} \\ DWF_f^- &= \frac{\phi_f - \phi_F}{\phi_C - \phi_F} \end{aligned} \tag{12.82}$$

Table 12.1 Functional relationships of the DWF_f for some HO and HR schemes on uniform grid

Scheme	Downwind weighing factor-NVF
Upwind	$DWF_f = 0$
SOU	$DWF_f = \dfrac{\tilde{\phi}_C}{2\left(1-\tilde{\phi}_C\right)}$
CD	$DWF_f = \dfrac{1}{2}$
FROMM	$DWF_f = \dfrac{1}{4\left(1-\tilde{\phi}_C\right)}$
QUICK	$DWF_f = \dfrac{1}{4} + \dfrac{1}{8\left(1-\tilde{\phi}_C\right)}$
Downwind	$DWF_f = 1$
MINMOD	$DWF_f = \begin{cases} \dfrac{1}{2}\dfrac{\tilde{\phi}_C}{\left(1-\tilde{\phi}_C\right)} & 0 \le \tilde{\phi}_C \le \dfrac{1}{2} \\ \dfrac{1}{2} & \dfrac{1}{2} \le \tilde{\phi}_C \le 1 \\ 0 & elsewhere \end{cases}$
Bounded CD	$DWF_f = \begin{cases} \dfrac{1}{2} & 0 \le \tilde{\phi}_C \le 1 \\ 0 & elsewhere \end{cases}$
OSHER [30]	$DWF_f = \begin{cases} \dfrac{1}{2}\dfrac{\tilde{\phi}_C}{\left(1-\tilde{\phi}_C\right)} & 0 \le \tilde{\phi}_C \le \dfrac{2}{3} \\ 1 & \dfrac{2}{3} \le \tilde{\phi}_C \le 1 \\ 0 & elsewhere \end{cases}$
SMART	$DWF_f = \begin{cases} \dfrac{2\tilde{\phi}_C}{1-\tilde{\phi}_C} & 0 \le \tilde{\phi}_C \le \dfrac{1}{6} \\ \dfrac{1}{4} + \dfrac{1}{8\left(1-\tilde{\phi}_C\right)} & \dfrac{1}{6} \le \tilde{\phi}_C \le \dfrac{5}{6} \\ 1 & \dfrac{5}{6} \le \tilde{\phi}_C \le 1 \\ 0 & elsewhere \end{cases}$
STOIC	$DWF_f = \begin{cases} \dfrac{2\tilde{\phi}_C}{1-\tilde{\phi}_C} & 0 \le \tilde{\phi}_C \le \dfrac{1}{5} \\ \dfrac{1}{2} & \dfrac{1}{5} \le \tilde{\phi}_C \le \dfrac{1}{2} \\ \dfrac{1}{4} + \dfrac{1}{8\left(1-\tilde{\phi}_C\right)} & \dfrac{1}{2} \le \tilde{\phi}_C \le \dfrac{5}{6} \\ 1 & \dfrac{5}{6} \le \tilde{\phi}_C \le 1 \\ 0 & elsewhere \end{cases}$
MUSCL	$DWF_f = \begin{cases} \dfrac{\tilde{\phi}_C}{1-\tilde{\phi}_C} & 0 \le \tilde{\phi}_C \le \dfrac{1}{4} \\ \dfrac{1}{4\left(1-\tilde{\phi}_C\right)} & \dfrac{1}{4} \le \tilde{\phi}_C \le \dfrac{3}{4} \\ 1 & \dfrac{3}{4} \le \tilde{\phi}_C \le 1 \\ 0 & elsewhere \end{cases}$

The fluxes in Eq. (12.77) can now be expressed as

$$\begin{aligned} FluxF_f &= \left\|\dot{m}_f, 0\right\| DWF_f^+ - \left\|-\dot{m}_f, 0\right\| \left(1 - DWF_f^-\right) \\ FluxC_f &= \left\|\dot{m}_f, 0\right\| \left(1 - DWF_f^+\right) - \left\|-\dot{m}_f, 0\right\| DWF_f^- \end{aligned} \tag{12.83}$$

and the discretized equation becomes

$$a_C \phi_C + \sum_{F \sim NB(C)} a_F \phi_F = b_C \tag{12.84}$$

with

$$\begin{aligned} a_F &= FluxF_f \\ a_C &= \sum_{f \sim nb(C)} FluxC_f = -\sum_{F \sim NB(C)} a_F + \sum_{f \sim nb(C)} \dot{m}_f \\ b_C &= Q_C^{\phi} V_C \end{aligned} \tag{12.85}$$

The coefficients in Eq. (12.85) result in a highly unstable system of equations, thus requiring substantial relaxation. This can be demonstrated on a simple one-dimensional mesh (Fig. 12.8). Without loss of generality, a positive flow field is assumed, which reduces Eq. (12.84) to

$$a_C \phi_C + a_E \phi_E + a_W \phi_W = b_C \tag{12.86}$$

where

$$\begin{aligned} a_E &= FluxF_e = \dot{m}_e DWF_e^+ \\ a_W &= FluxF_w = \dot{m}_w \left(1 - DWF_w^-\right) \\ a_C &= \sum_{f \sim nb(C)} FluxC_f = -\left[\dot{m}_e DWF_e^+ + \dot{m}_w \left(1 - DWF_w^-\right)\right] + \dot{m}_e + \dot{m}_w \end{aligned} \tag{12.87}$$

The continuity constraint implies that

$$\dot{m}_e + \dot{m}_w = 0 \Rightarrow \dot{m}_w = -\dot{m}_e \tag{12.88}$$

thus the coefficients become

$$\begin{aligned} a_E &= FluxF_e = \dot{m}_e DWF_e^+ \\ a_W &= FluxF_w = -\dot{m}_e \left(1 - DWF_w^-\right) \\ a_C &= \sum_{f \sim nb(C)} FluxC_f = -\dot{m}_e \left[DWF_e^+ + DWF_w^- - 1\right] \end{aligned} \tag{12.89}$$

In the above equation the a_E and a_W coefficients have opposite signs, a violation to one of the basic coefficient rules. Furthermore for values of the *DWF* factors that are larger than 0.5 (i.e., $DWF > 0.5$), the diagonal coefficient a_C becomes negative resulting in a system not solvable by iterative means. This would occur whenever $\phi_f > 0.5(\phi_C + \phi_D)$ a situation common to all HR schemes for $\phi_C > 0.5$. In fact the DWF moves much of the HR flux influence onto the downwind value causing the above mentioned issues, a situation that resembles in effect the central difference scheme.

12.8.2 The Normalized Weighing Factor (NWF) Method

The Normalized Weighing Factor (NWF) method was developed [29] to address the shortcomings of the DWF method. It operates by linearizing the normalized interpolation profile such that

$$\tilde{\phi}_f = \ell \tilde{\phi}_C + k \tag{12.90}$$

where ℓ and k are constants that represent the slope and intercept of the linear function within any interval of ϕ_f, with the number of intervals depending on the HR scheme used. This is an exact representation for nearly all HR schemes.

For example, by equating Eq. (12.90) to the NVF form of the MINMOD scheme (Eq. 12.14), the values of ℓ and k are deduced to be

$$[\ell, k] = \begin{cases} \left[\frac{3}{2}, 0\right] & 0 < \tilde{\phi}_C < \frac{1}{2} \\ \left[\frac{1}{2}, \frac{1}{2}\right] & \frac{1}{2} \le \tilde{\phi}_C < 1 \\ [1, 0] & \textit{elsewhere} \end{cases} \tag{12.91}$$

In a second step Eq. (12.90) is rewritten as

$$\frac{\phi_f - \phi_U}{\phi_D - \phi_U} = \ell \frac{\phi_C - \phi_U}{\phi_D - \phi_U} + k \tag{12.92}$$

and transformed to

$$\phi_f = \ell(\phi_C - \phi_U) + k(\phi_D - \phi_U) + \phi_U = \ell\phi_C + k\phi_D + (1 - \ell - k)\phi_U \tag{12.93}$$

where ϕ_U, ϕ_D, and ϕ_C are the values at the U, D, and C nodes whose locations depend on the flow direction. The values of ℓ and k for a number of HO and HR schemes are listed in Table 12.2 (for unstructured and/or structured uniform grid).

Since for an unstructured grid the U location is virtual, the term involving ϕ_U is treated in a deferred correction fashion. However the value of the resulting deferred

Table 12.2 NVF values of NWF $[\ell, k]$ factors for some HO and HR schemes

Scheme	Uniform grid (NVF)
Upwind	$[\ell, k] = [1, 0]$
SOU	$[\ell, k] = \left[\frac{3}{2}, 0\right]$
CD	$[\ell, k] = \left[\frac{1}{2}, \frac{1}{2}\right]$
FROMM	$[\ell, k] = \left[1, \frac{1}{4}\right]$
QUICK	$[\ell, k] = \left[\frac{3}{4}, \frac{3}{8}\right]$
MINMOD	$[\ell, k] = \begin{cases} \left[\frac{3}{2}, 0\right] & 0 < \tilde{\phi}_C < \frac{1}{2} \\ \left[\frac{1}{2}, \frac{1}{2}\right] & \frac{1}{2} \le \tilde{\phi}_C < 1 \\ [1, 0] & elsewhere \end{cases}$
OSHER	$[\ell, k] = \begin{cases} \left[\frac{3}{2}, 0\right] & 0 < \tilde{\phi}_C < \frac{2}{3} \\ [0, 1] & \frac{2}{3} \le \tilde{\phi}_C < 1 \\ [1, 0] & elsewhere \end{cases}$
MUSCL	$[\ell, k] = \begin{cases} [2, 0] & 0 < \tilde{\phi}_C < \frac{1}{4} \\ \left[1, \frac{1}{4}\right] & \frac{1}{4} \le \tilde{\phi}_C < \frac{3}{4} \\ [0, 1] & \frac{3}{4} \le \tilde{\phi}_C < 1 \\ [1, 0] & elsewhere \end{cases}$
SMART	$[\ell, k] = \begin{cases} [4, 0] & 0 < \tilde{\phi}_C < \frac{1}{6} \\ \left[\frac{3}{4}, \frac{3}{8}\right] & \frac{1}{6} \le \tilde{\phi}_C < \frac{5}{6} \\ [0, 1] & \frac{5}{6} \le \tilde{\phi}_C < 1 \\ [1, 0] & elsewhere \end{cases}$

correction source term (i.e., $(1 - \ell - k)\phi_U \, l \ge 0, k \ge 0$) is smaller than the one that would be obtained with the standard deferred correction treatment (i.e., ϕ_U). Thus the NWF requires less under-relaxation than the standard DC method and thus allows for faster convergence.

Starting with Eq. (12.93), the convection flux in the general case (i.e., multi dimensional unstructured grid) can be written in the form

$$\begin{aligned} \dot{m}_f \phi_f = & \| \dot{m}_f, 0 \| \left[\ell_f^+ \phi_C + k_f^+ \phi_F + \left(1 - \ell_f^+ - k_f^+\right) \phi_U^+ \right] \\ & - \| -\dot{m}_f, 0 \| \left[\ell_f^- \phi_F + k_f^- \phi_C + \left(1 - \ell_f^- - k_f^-\right) \phi_U^- \right] \end{aligned} \tag{12.94}$$

and linearized to yield

$$\begin{aligned} FluxF_f &= \|\dot{m}_f, 0\|\, k_f^+ - \|-\dot{m}_f, 0\|\, \ell_f^- \\ FluxC_f &= \|\dot{m}_f, 0\|\, \ell_f^+ - \|-\dot{m}_f, 0\|\, k_f^- \\ FluxV_f &= \|\dot{m}_f, 0\| \left(1 - \ell_f^+ - k_f^+\right)\phi_U^+ - \|-\dot{m}_f, 0\| \left(1 - \ell_f^- - k_f^-\right)\phi_U^- \end{aligned} \tag{12.95}$$

Substituting Eq. (12.95) into Eq. (12.77) the algebraic equation is obtained as

$$a_C\phi_C + \sum_{F\sim NB(C)} a_F\phi_F = b_C \tag{12.96}$$

where now

$$\begin{aligned} a_F &= FluxF_f = k_f^+\|\dot{m}_f, 0\| - \ell_f^-\|-\dot{m}_f, 0\| \\ a_C &= \sum_{f\sim nb(C)} FluxC_f = \sum_{f\sim nb(C)} \left(\ell_f^+\|\dot{m}_f, 0\| - k_f^-\|-\dot{m}_f, 0\|\right) \\ b_C &= Q_C^\phi V_C - \underbrace{\sum_{f\sim nb(C)} FluxV_f}_{b_C^{DC}} \\ &= Q_C^\phi V_C - \underbrace{\sum_{f-nb(C)} \left[\left(1 - \ell_f^+ - k_f^+\right)\phi_U^+\|\dot{m}_f, 0\| - \left(1 - \ell_f^- - k_f^-\right)\phi_U^-\|-\dot{m}_f, 0\|\right]}_{b_C^{DC}} \end{aligned} \tag{12.97}$$

The NWF was originally developed for use on structured grids with its formulation in that context allowing for a full implicit treatment of HR schemes. The full implicitness of the method on structured grid is the result of ϕ_U being an actual node in the computational domain that can be resolved in the algebraic equation, which now has a larger stencil that includes the far nodes *EE* and *WW*. For the one dimensional structured grid displayed in Fig. 12.8, the NWF form of the algebraic equation becomes

$$a_C\phi_C + \sum_{F\sim E,W,EE,WW} a_F\phi_F = b_C \tag{12.98}$$

where

$$\begin{aligned} a_E &= FluxF_e = \|\dot{m}_e, 0\|k_e^+ - \|-\dot{m}_e, 0\|\ell_e^- + \|\dot{m}_w, 0\|\left(1 - \ell_w^+ - k_w^+\right) \\ a_W &= FluxF_w = \|\dot{m}_w, 0\|k_w^+ - \|-\dot{m}_w, 0\|\ell_w^- + \|\dot{m}_e, 0\|\left(1 - \ell_e^+ - k_e^+\right) \\ a_{EE} &= FluxF_{ee} = -\|-\dot{m}_e, 0\|\left(1 - \ell_e^- - k_e^-\right) \\ a_{WW} &= FluxF_{ww} = -\|-\dot{m}_w, 0\|\left(1 - \ell_w^- - k_w^-\right) \\ a_C &= \sum_{f\sim nb(C)} FluxC_f = \|\dot{m}_e, 0\|\ell_e^+ + \|\dot{m}_w, 0\|\ell_w^+ - \|-\dot{m}_e, 0\|k_e^- - \|-\dot{m}_w, 0\|k_w^- \\ &= -(a_E + a_W + a_{EE} + a_{WW}) + (\dot{m}_e + \dot{m}_w) \end{aligned} \tag{12.99}$$

In the NWF reformulation of the HR schemes since the value of ℓ is greater than that of k (see Fig. 12.6), except in a narrow region of the NVD close to the Downwind line as explained next, the value of a_C is always positive and instability does not arise. Along the Downwind line of the NVD, where $(\ell, k) = (0, 1)$, a value of zero for the a_C coefficient is obtained. In this case (ℓ, k) is set to $\left(L, 1 - L\phi_f\right)$ where L is usually set to the value of ℓ in the previous interval of the composite scheme.

This basically allows the NWF to be much more robust than the DWF as it guarantees positive a_C coefficients.

12.8.2.1 The NWF Method in the Context of the TVD

With the exception of the MUSCL Van Leer limiter, the limiters of the TVD formulation of all HR schemes presented earlier appear as straight lines on Sweby's diagram and as such can be written as a set of linear equations of the form

$$\psi\left(r_f\right) = mr_f + n \tag{12.100}$$

where m and n are constants (slope and intercept of the linear function and depend on geometric quantities only) within any interval of $\psi\left(r_f\right)$, with the number of intervals depending on the HR TVD scheme used. For example, by equating Eq. (12.100) to the TVD form of the MINMOD scheme (Eq. 12.44), the values of m and n are deduced to be

$$\text{MINMOD} \quad [m, n] = \begin{cases} [1, 0] & 0 < r_f < 1 \\ [0, 1] & r_f \geq 1 \\ [0, 0] & r_f \leq 0 \end{cases} \tag{12.101}$$

Substituting Eq. (12.100) in Eq. (12.30), the interface value is found to be

$$\begin{aligned} \phi_f &= \phi_C + \frac{1}{2}\left(mr_f + n\right)\left(\phi_D - \phi_C\right) \\ &= \phi_C + \frac{1}{2}\left(m\frac{\phi_C - \phi_U}{\phi_D - \phi_C} + n\right)\left(\phi_D - \phi_C\right) \\ &= \left(1 + \frac{1}{2}m - \frac{1}{2}n\right)\phi_C + \frac{1}{2}n\phi_D - \frac{1}{2}m\phi_U \end{aligned} \tag{12.102}$$

where ϕ_U, ϕ_D, and ϕ_C are again the values at the U, D, and C nodes whose locations depend on the flow direction. The values of m and n for a number of HO and HR schemes are listed in Table 12.3 for uniform grids. Moreover Eq. (12.102) has the same form as Eq. (12.93) with

$$\ell = 1 + \frac{1}{2}m - \frac{1}{2}n \quad \text{and} \quad k = \frac{1}{2}n \tag{12.103}$$

Thus an approach similar to that of the NVF-NWF can be used for the implementation of the TVD-NWF.

Table 12.3 TVD values of NWF $[m,n]$ factors for some HO and HR schemes

Scheme	Uniform grid (NVF)
Upwind	$[m,n]=[0,0]$
SOU	$[m,n]=[1,0]$
CD	$[m,n]=[0,1]$
FROMM	$[m,n]=\left[\frac{1}{2},\frac{1}{2}\right]$
QUICK	$[m,n]=\left[\frac{1}{4},\frac{3}{4}\right]$
DOWNWIND	$[m,n]=[0,2]$
OSHER	$[m,n]=\begin{cases}[1,0] & 0<r_f<2\\ [0,2] & r_f\geq 2\\ [0,0] & r\leq 0\end{cases}$
MUSCL	$[m,n]=\begin{cases}[2,0] & 0<r_f<\frac{1}{3}\\ \left[\frac{1}{2},\frac{1}{2}\right] & \frac{1}{3}\leq r_f<3\\ [0,2] & r_f\geq 3\\ [0,0] & r_f\leq 0\end{cases}$
SUPERBEE	$[m,n]=\begin{cases}[2,0] & 0<r_f<\frac{1}{2}\\ [0,1] & \frac{1}{2}\leq r_f<1\\ [1,0] & 1\leq r_f<2\\ [0,2] & r_f\geq 2\\ [0,0] & r_f\leq 0\end{cases}$

12.9 Boundary Conditions

The Boundary conditions for the convection term are generally much simpler than for the diffusion term. The particulars of the implementation of the following boundary conditions: "Inlet", "Outlet", "Wall", and "Symmetry" are now detailed.

Typical boundary elements are shown in Fig. 12.17. A boundary cell, as mentioned earlier in this book, is one that has one or more faces on the boundary. Discrete values of ϕ are stored both at centroids of boundary cells and of boundary faces.

Let C denotes the centroid of the boundary element with one boundary face of centroid b and of surface vector $\mathbf{S}_b$ pointing outward (Fig. 12.17). As before, the discretization process over cell C of a pure convection problem in a multidimensional domain yields

$$\sum_{f\sim nb(C)}\left(\mathbf{J}^{\phi,C}\cdot\mathbf{S}\right)_f=0 \tag{12.104}$$

The fluxes on the interior faces are discretized as before. Independent of the boundary condition type, the boundary flux $\mathbf{J}_b^{\phi,C}$ may be written using the boundary face centroid value as

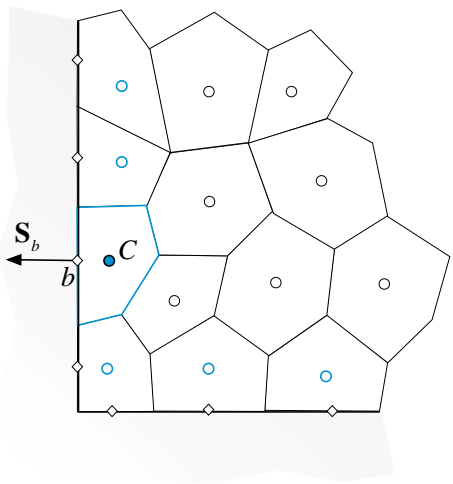

Fig. 12.17 Boundary elements with one or two boundary faces

$$\mathbf{J}_b^{\phi,C} = (\rho \mathbf{v}\phi)_b \tag{12.105}$$

such that

$$\mathbf{J}_b^{\phi,C} \cdot \mathbf{S}_b = (\rho \mathbf{v}\phi)_b \cdot \mathbf{S}_b = \dot{m}_b \phi_b \tag{12.106}$$

Thus the discretized equation of the boundary cell is expressed as

$$\sum_{f \sim nb(C)} (\rho \mathbf{v}\phi \cdot \mathbf{S})_f + (\rho \mathbf{v}\phi \cdot \mathbf{S})_b = 0 \tag{12.107}$$

where subscript f refers to interior faces and subscript b to the boundary face. The specification of boundary conditions involves either specifying the unknown boundary value ϕ_b, or alternatively, the boundary flux $\mathbf{J}_b^{\phi,C}$. Using Eq. (12.107), the discretized equations at a boundary element for the different boundary condition types of convection problems are derived next.

12.9.1 Inlet Boundary Condition

At inlet to a domain (Fig. 12.18), the value of ϕ is usually specified. Since the velocity field is assumed to be known, then the convective flux at inlet is also known. Therefore the boundary flux is moved to the right hand side and treated as a source term. With this modification Eq. (12.107) becomes

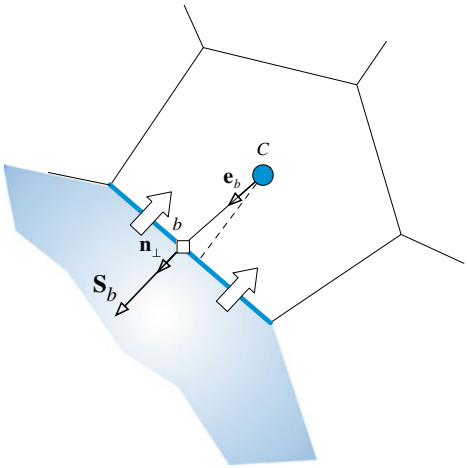

Fig. 12.18 Inlet boundary condition for the convection flux

$$\sum_{f\sim nb(C)} (\rho \mathbf{v}\cdot\mathbf{S})_f \phi_f = -(\rho \mathbf{v}\cdot\mathbf{S})_b \phi_b = -\dot{m}_b \phi_b \tag{12.108}$$

If a HR scheme is used to discretize the convection flux at interior faces and is implemented via a deferred correction approach, then the modified algebraic equation for the boundary element can be written as

$$a_C \phi_C + \sum_{F\sim NB(C)} a_F \phi_F = b_C \tag{12.109}$$

where

$$\begin{aligned} a_F &= FluxF_f = -\|-\dot{m}_f, 0\| \\ a_C &= \sum_{f\sim nb(C)} FluxC_f = \sum_{f\sim nb(C)} \|\dot{m}_f, 0\| \\ &= -\sum_{F\sim NB(C)} a_F + \sum_{f\sim nb(C)} \dot{m}_f \\ b_C &= -\sum_{f\sim nb(C)} FluxV_f = -\dot{m}_b \phi_b - \underbrace{\sum_{f\sim nb(C)} \dot{m}_f \left(\phi_f^{HR} - \phi_f^U\right)}_{b_c^{DC}} \end{aligned} \tag{12.110}$$

where F refers to interior neighboring nodes of the C grid point and f refers to interior faces of the boundary element.

12.9.2 Outlet Boundary Condition

At outlet from the domain (Fig. 12.19) no information downstream of the boundary grid point is available. However, being a directional phenomenon, the value of ϕ at the boundary is highly dependent on upstream locations. In fact, the upwind and SOU schemes, for example, do not require any information at outlet since its value can be expressed as a function of values at upstream nodes. The treatment that has proven to be very effective at an outlet boundary condition is to assume the ϕ profile to be fully developed, which is equivalent to assuming that the normal gradient to the face is zero [i.e., $(\nabla\phi \cdot \mathbf{n})_b = (\partial\phi/\partial n)_b = 0$]. The usual practice at an outlet (Fig. 12.19) is to apply the upwind scheme ($\phi_b = \phi_C$), which automatically results in a zero normal gradient.

Discretizing the convection flux at interior faces using a HR scheme implemented through a deferred correction approach, the modified algebraic equation for the boundary element can be written as

$$a_C\phi_C + \sum_{F\sim NB(C)} a_F\phi_F = b_C \tag{12.111}$$

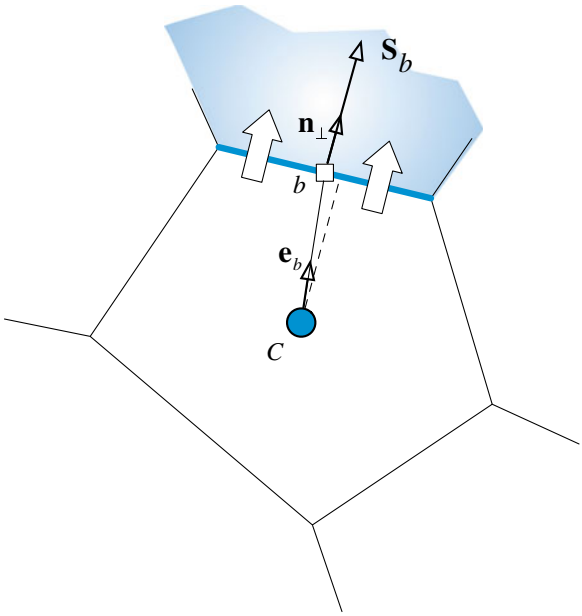

Fig. 12.19 Outlet boundary condition for the convection flux

where

$$\begin{aligned} a_F &= FluxF_f = -\,\|-\dot{m}_f, 0\,\| \\ a_C &= \sum_{f\sim nb(C)} FluxC_f = \sum_{f\sim nb(C)} \|\dot{m}_f, 0\,\| \\ &= -\sum_{F\sim NB(C)} a_F + \sum_{f\sim nb(C)} \left(\dot{m}_f + \dot{m}_b\right) \\ b_C &= -\sum_{f\sim nb(C)} FluxV_f = \underbrace{-\sum_{f\sim nb(C)} \dot{m}_f \left(\phi_f^{HR} - \phi_f^{U}\right)}_{b_c^{DC}} \end{aligned} \tag{12.112}$$

where f refers to the interior faces of the boundary element, and C and F refer to owner and neighbor, respectively.

12.9.3 Wall Boundary Condition

As shown in Fig. 12.20, the normal velocity at a wall is zero. As such the convection flux is zero and does not appear in the algebraic equation.

Again adopting a HR scheme with a deferred correction approach, the modified algebraic equation for the boundary element can be written as

$$a_C\phi_C + \sum_{F\sim NB(C)} a_F\phi_F = b_C \tag{12.113}$$

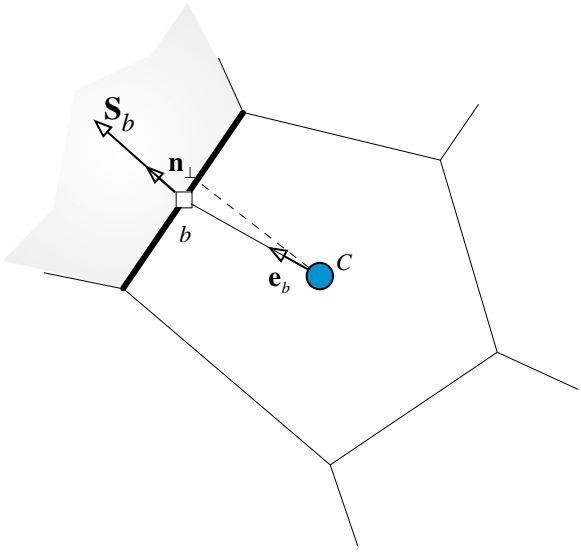

Fig. 12.20 Wall boundary condition for the convection flux

where

$$\begin{aligned} a_F &= FluxF_f = -\|-\dot{m}_f, 0\| \\ a_C &= \sum_{f\sim nb(C)} FluxC_f = \sum_{f\sim nb(C)} \|\dot{m}_f, 0\| \\ &= -\sum_{F\sim NB(C)} a_F + \sum_{f\sim nb(C)} \dot{m}_f \\ b_C &= -\sum_{f\sim nb(C)} FluxV_f = \underbrace{-\sum_{f\sim nb(C)} \dot{m}_f \left(\phi_f^{HR} - \phi_f^U\right)}_{b_c^{DC}} \end{aligned} \tag{12.114}$$

Again f refers to the interior faces of the boundary element and C and F refer to the owner and neighbor nodes, respectively.

12.9.4 Symmetry Boundary Condition

No flow crosses a symmetry boundary. Therefore it is treated in a similar fashion to a wall boundary condition with the convection flux normal to a symmetry boundary set to zero.

12.10 Computational Pointers

12.10.1 uFVM

Similar to HO schemes discussed in Chap. 11, HR schemes are implemented in uFVM using the deferred correction method. The main difference in the implementation stems from the use of the NVF or TVD relations rather than the calculation of the face value using directly the gradient. The implementation of the STOIC HR [31] scheme using the NVF formulation is shown in Listing 12.1 (cfdAssembleConvectionTermDCSTOIC).

It starts with the retrieval of the needed fields, followed by setting the upwind and downing indices for all interior faces. Then for each face, ϕ_C and ϕ_D are identified, ϕ_U is constructed, and $\tilde{\phi}_C$ is computed and used to calculate the face value from the NVF relationship of the adopted HR scheme. Finally ϕ_f is reconstructed from $\tilde{\phi}_f$ and used in the deferred correction method.

```
theFluidTag = cfdGetFluidTag(theEquationName);
theMdotName = ['Mdot' theFluidTag];
theMdotField = cfdGetMeshField(theMdotName,'Faces');
mdot_f = theMdotField.phi(iFaces);

iOwners = [theMesh.faces(iFaces).iOwner]';
iNeighbours = [theMesh.faces(iFaces).iNeighbour]';
pos = zeros(size(mdot_f));
pos(mdot_f>0)=1;

% find indices of U and D cells
iUpwind   =  pos   .*iOwners + (1-pos).*iNeighbours;
iDownwind = (1-pos).*iOwners +  pos   .*iNeighbours;

% find phi_C, phi_D and calculate phi_U
phi_C = phi(iUpwind,iComponent);
phi_D = phi(iDownwind,iComponent);
rCD                    =       [theMesh.elements(iDownwind).centroid]'-
[theMesh.elements(iUpwind).centroid]';

phi_U = phi_D - 2*dot(phiGrad(iUpwind,:,iComponent)',rCD')';

SMALL= 1e-6;
% calculate phi_tildaC
nominator = phi_C-phi_U;
denominator = phi_D-phi_U;
divideLoc = find(~((denominator<SMALL) & (denominator>-SMALL)));
phi_tildaC = ones(size(phi_C));
phi_tildaC(divideLoc) = nominator(divideLoc)./denominator(divideLoc);
```

Listing 12.1 Implementation of the STOIC HR scheme

```
% get phi_tildaf from STOIC function
phi_tildaf = zeros(size(phi_tildaC));
% lower UPWIND section
phi_tildaf       =       phi_tildaf       +       (phi_tildaC       <=
0)                     .*(phi_tildaC);
% intermediate section
phi_tildaf  =  phi_tildaf  +  (phi_tildaC  >  0)       .*(phi_tildaC  <
0.2).*(3*phi_tildaC);
% CDS section
phi_tildaf   =   phi_tildaf   +   (phi_tildaC   >=   0.2).*(phi_tildaC   <
0.5).*(0.5*phi_tildaC + 0.5);
% SMART section
phi_tildaf   =   phi_tildaf   +   (phi_tildaC   >=   0.5).*(phi_tildaC   <
5/6).*(0.75*phi_tildaC + 3/8);
% DOWNWIND section
phi_tildaf   =   phi_tildaf   +   (phi_tildaC   >=   5/6).*(phi_tildaC   <
1)  .*(ones(size(phi_tildaC)));
% upper UPWIND section
phi_tildaf       =       phi_tildaf       +       (phi_tildaC       >=
1)                     .*(phi_tildaC);


% calculate phi_f
phi_f = phi_tildaf.*(phi_D-phi_U) + phi_U;


% calculate correction
corr = mdot_f .* (phi_f - phi_C);


% apply deferred correction
theFluxes.FLUXTf(iFaces) = theFluxes.FLUXTf(iFaces) + corr;
```

Listing 12.1 (continued)

12.10.2 OpenFOAM®

As discussed in Chap. 11 the discretization of the convection term in OpenFOAM® [32] is accomplished through the base class **surfaceInterpolationScheme**. This class is inherited by any face interpolation algorithm. High resolution schemes, as discussed in this chapter, are special face interpolation algorithms. Thus, as displayed in Fig. 12.21, OpenFOAM® groups all TVD schemes in a base class, derived from the **surfaceInterpolationScheme** class, denoted by the **limitedSurfaceInterpolationScheme** class.

As shown in Listing 12.2, this class consists of the following three main functions: the virtual **weights** function representing the main virtual function of the **surfaceInterpolationScheme** class, a local **weights** function defined with three arguments, and a new virtual base function called **limiter**.

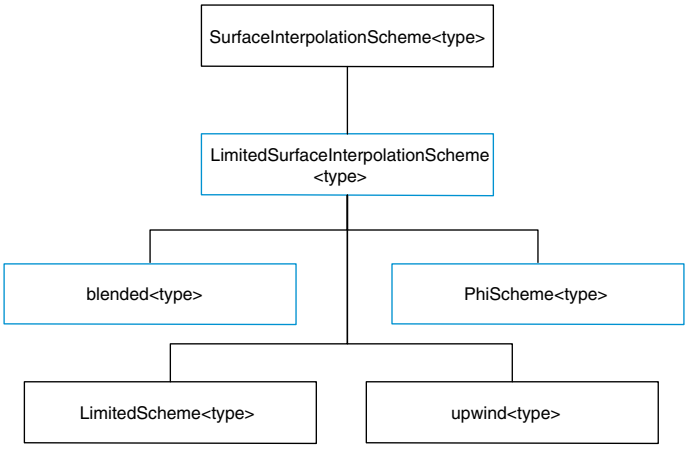

Fig. 12.21 UML showing the base class that groups all TVD schemes

```
template<class Type>
class limitedSurfaceInterpolationScheme
:
    public surfaceInterpolationScheme<Type>
{
…
// Member Functions
 //- Returns the interpolation weighting factors
 virtual tmp<surfaceScalarField> limiter
 (
     const GeometricField<Type, fvPatchField, volMesh>&
 ) const = 0;
 //- Returns the interpolation weighting factors for the given
 //  field, by limiting the given weights with the given limiter
 tmp<surfaceScalarField> weights
 (
     const GeometricField<Type, fvPatchField, volMesh>&,
     const surfaceScalarField& CDweights,
     tmp<surfaceScalarField> tLimiter
 ) const;
 //- Return the interpolation weighting factors for the given field
 virtual tmp<surfaceScalarField> weights
 (
     const GeometricField<Type, fvPatchField, volMesh>&
 ) const;
```

Listing 12.2 The **limitedSurfaceInterpolationScheme** class showing its three main functions

The script of the virtual **weights** function, shown in Listing 12.3, is given by

```
template<class Type>
tmp<surfaceScalarField>
limitedSurfaceInterpolationScheme<Type>::weights
(
    const GeometricField<Type, fvPatchField, volMesh>& phi
```

Listing 12.3 Script showing the implementation of the virtual **weights** function

```
        ) const
        {
            return this->weights
            (
                phi,
                this->mesh().surfaceInterpolation::weights(),
                this->limiter(phi)
            );
        }
```

Listing 12.3 (continued)

It is clear that executing the script instantiates the additional local **weights** function. The three main arguments of the local **weights** function are the flux **phi**, the linear interpolation **weights** (representing the central differencing weights), and the returning object of the virtual base class **limiter**. These are clearly shown in Listing 12.4 where the local **weights** function is defined.

```
template<class Type>
tmp<surfaceScalarField>
limitedSurfaceInterpolationScheme<Type>::weights
(
    const GeometricField<Type, fvPatchField, volMesh>& phi,
    const surfaceScalarField& CDweights,
    tmp<surfaceScalarField> tLimiter
) const
{
    surfaceScalarField& Weights = tLimiter();
    scalarField& pWeights = Weights.internalField();
    forAll(pWeights, face)
    {
        pWeights[face] =
            pWeights[face]*CDweights[face]
          + (1.0 - pWeights[face])*pos(faceFlux_[face]);
    }
```

Listing 12.4 Script showing the implementation of the local **weights** function

The calculation of the interpolation weights according to the TVD formulation implemented in Listing 12.4 may seem, from a first look, a bit unclear. Confusion may be eliminated by considering the case of a positive flux, for example, for which the weight ϖ is calculated as

$$\varpi = \varpi_{CD}\psi + (1 - \psi) \tag{12.115}$$

For a uniform grid $\varpi_{CD} = 1/2$ yielding

$$\varpi = \frac{\psi}{2} + (1 - \psi) = 1 - \frac{\psi}{2} \tag{12.116}$$

Recalling Eq. (11.164) and substituting the weight yields

$$\phi_f = \phi_N + \varpi(\phi_O - \phi_N) = \phi_N + \left(1 - \frac{\psi}{2}\right)(\phi_O - \phi_N) = \phi_O + \frac{\psi}{2}(\phi_N - \phi_O) \tag{12.117}$$

which is Eq. (12.30) in the TVD formulation.

So far the implementation of HR schemes in OpenFOAM® following the TVD formulation has been discussed along with its integration in the standard convection discretization procedure by properly defining the interpolation weights. Due to the many TVD schemes that can be used, OpenFOAM® has introduced a base virtual function denoted by **limiter** for the implementation of these schemes. The last step of the computational pointer is to describe how this class is defined and which classes, this **limiter** base class, engage.

All TVD limiters are organized through a class named **LimitedScheme** that inherits and defines the **limiter** function of the **limitedSurfaceInterpolation Scheme** class. The definition of this class is based on nested template classes definition in which the derived class is described with a template argument, as shown in Listing 12.5.

```
template<class Type, class Limiter, template<class> class LimitFunc>
class LimitedScheme
:
    public limitedSurfaceInterpolationScheme<Type>,
    public Limiter
{
…
```

Listing 12.5 The **LimitedScheme** class with the **Limiter** template

Here **Limiter** is not a function but just a template definition. Additionally the virtual **limiter** class is now specialized (Listing 12.6).

```
//- Return the interpolation weighting factors
 virtual tmp<surfaceScalarField> limiter
 (
     const GeometricField<Type, fvPatchField, volMesh>&
 ) const;
```

Listing 12.6 The virtual **limiter** class

As depicted in Listing 12.7 the definition of the **limiter** function is practically linked to an auxiliary function named **calcLimiter**.

```
 template<class Type, class Limiter, template<class> class LimitFunc>
Foam::tmp<Foam::surfaceScalarField>
Foam::LimitedScheme<Type, Limiter, LimitFunc>::limiter
(
    const GeometricField<Type, fvPatchField, volMesh>& phi
) const
{
…
       tmp<surfaceScalarField> tlimiterField
        (
            new surfaceScalarField
            (
                IOobject
                (
                    limiterFieldName,
                    mesh.time().timeName(),
                    mesh
                ),
                mesh,
                dimless
            )
        );
```

Listing 12.7 The script used to call the **calcLimiter** function

```
        calcLimiter(phi, tlimiterField());

        return tlimiterField;
…
```

Listing 12.7 (continued)

The core of the **calcLimiter** function is to evaluate the TVD limiter and to store it in the **tlimiterField**, as shown in Listings 12.7 and 12.8.

```
template<class Type, class Limiter, template<class> class LimitFunc>
void Foam::LimitedScheme<Type, Limiter, LimitFunc>::calcLimiter
(
    const GeometricField<Type, fvPatchField, volMesh>& phi,
    surfaceScalarField& limiterField
) const
{
    const fvMesh& mesh = this->mesh();


         tmp<GeometricField<typename  Limiter::phiType,  fvPatchField,
volMesh> >
        tlPhi = LimitFunc<Type>()(phi);


       const  GeometricField<typename  Limiter::phiType,  fvPatchField,
volMesh>&
        lPhi = tlPhi();


      tmp<GeometricField<typename  Limiter::gradPhiType,  fvPatchField,
volMesh> >
        tgradc(fvc::grad(lPhi));
     const GeometricField<typename Limiter::gradPhiType, fvPatchField,
volMesh>&
        gradc = tgradc();


                    const      surfaceScalarField&      CDweights      =
mesh.surfaceInterpolation::weights();
```

Listing 12.8 Script used with the **calcLimiter** function

```
    const labelUList& owner = mesh.owner();
    const labelUList& neighbour = mesh.neighbour();

    const vectorField& C = mesh.C();

    scalarField& pLim = limiterField.internalField();

    forAll(pLim, face)
    {
       label own = owner[face];
       label nei = neighbour[face];
       pLim[face] = Limiter::limiter
       (
           CDweights[face],
           this->faceFlux_[face],
           lPhi[own],
           lPhi[nei],
           gradc[own],
           gradc[nei],
           C[nei] - C[own]
       );
    }
```

Listing 12.8 (continued)

In the **calcLimiter** function the following steps are performed:

- Storing a copy of the field to be interpolated in *lPhi*
- Evaluating the gradient of the lPhi field using fvc::grad(lPhi)
- Collecting the central differencing weights
- Collecting the cell centers
- Evaluating the limiter by calling the nested template class: **pLim [face] = Limiter::limiter**.

As an example of a Limiter::limiter function, the TVD formulation of the SUPERBEE given in Eq. (12.44) is considered. The OpenFOAM® definition can be found in "$FOAM_SRC/finiteVolume/interpolation/surfaceInterpolation/limited Schemes/Super Bee/SuperBee.H" file. In this case the script of the **limiter** function is given in Listing (12.9) as

```
scalar limiter
(
    const scalar cdWeight,
    const scalar faceFlux,
    const typename LimiterFunc::phiType& phiP,
    const typename LimiterFunc::phiType& phiN,
    const typename LimiterFunc::gradPhiType& gradcP,
    const typename LimiterFunc::gradPhiType& gradcN,
    const vector& d
) const
{
    scalar r = LimiterFunc::r
    (
        faceFlux, phiP, phiN, gradcP, gradcN, d
    );

    return max(max(min(2*r, 1), min(r, 2)), 0);
}
```

Listing 12.9 The limiter function of the SuperBee scheme

where the arguments are as stated before including the gradients, the central differencing weights, etc., while the returned value follows exactly Eq. (12.44).

The r definition follows the same nested template class and the function itself is defined in the file "$FOAM_SRC/src/finiteVolume/interpolation/surface Interpolation/ limitedSchemes/LimitedScheme/NVDTVD.H" according to Eq. (12.66). The implementation details are given in Listing 12.10.

```
scalar r
(
   const scalar faceFlux,
   const scalar phiP,
   const scalar phiN,
   const vector& gradcP,
   const vector& gradcN,
   const vector& d
) const
{
```

Listing 12.10 Script used to calculate r

```
    scalar gradf = phiN - phiP;

    scalar gradcf;

    if (faceFlux > 0)
    {
        gradcf = d & gradcP;
    }
    else
    {
        gradcf = d & gradcN;
    }
...
    {
        return 2*(gradcf/gradf) - 1;
    }
}
```

Listing 12.10 (continued)

12.11 Closure

The chapter dealt with the bounding of HO convection schemes. This was accomplished by enforcing a convection boundedness criterion (CBC). The resulting HO bounded schemes were denoted by HR schemes. The Normalized Variable Formulation (NVF) and Total Variation Diminishing (TVD) approaches were introduced as frameworks for the development of HR schemes. Two techniques for the implementation of HO and HR schemes in structured and unstructured grids were introduced, namely the Downwind Weighing Factor (DWF) method and the Normalized Weighing Factor (NWF) method. The next chapter is devoted to the discretization of the unsteady term.

12.12 Exercises

Exercise 1

a. Starting with the NVF form of the SMART scheme derive its equivalent TVD form.
b. Starting with the TVD form of the OSHER scheme derive its equivalent NVF form.

Exercise 2

For non-uniform grids the equations for the various schemes become geometry dependent. This is also true for the point Q through which schemes have to pass to be second order accurate.

Find the coordinates of Q in the general case of a non-uniform grid.

Hint: define a normalized space variable as [33]

$$\tilde{x} = \frac{x - x_U}{x_D - x_U}$$

Exercise 3

Derive the DWF_f and NWF_f relationships of the OSHER and SMART schemes.

Exercise 4

For the one dimensional uniform mesh shown in Fig. 12.22, use the NVF-SMART, NVF-OSHER, QUICK, and SOU schemes to compute ϕ_f for the following situations:

a. $\phi_U = 30,\ \phi_C = 20,\ \phi_D = 10$
b. $\phi_U = 10,\ \phi_C = 5,\ \ \phi_D = 15$
c. $\phi_U = 30,\ \phi_C = 10,\ \phi_D = 5$
d. $\phi_U = 30,\ \phi_C = 25,\ \phi_D = 5$

Exercise 5

For the one dimensional mesh shown in Fig. 12.22, use the TVD-VanLeer and TVD-MINMOD schemes to compute ϕ_f for the following situations:

a. $\phi_U = 30,\ \phi_C = 20,\ \phi_D = 10$
b. $\phi_U = 10,\ \phi_C = 5,\ \ \phi_D = 15$
c. $\phi_U = 30,\ \phi_C = 10,\ \phi_D = 5$
d. $\phi_U = 30,\ \phi_C = 25,\ \phi_D = 5$

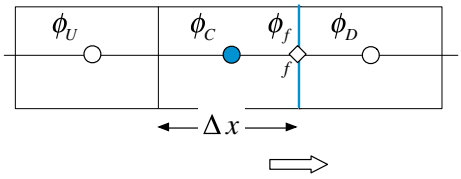

Fig. 12.22 A one dimensional uniform grid

Exercise 6

Consider the steady transport of a scalar ϕ in the domain shown in Fig. 12.23. The governing conservation equation is given by

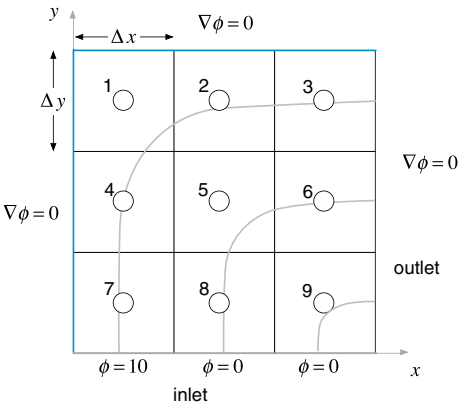

Fig. 12.23 Convection of a two dimensional scalar field

$$\nabla \cdot (\rho \mathbf{v} \phi) = 0$$

where $\rho = 1$, $\mathbf{v} = 2yx^2\mathbf{i} - 2xy^2\mathbf{j}$, and $\Delta x = \Delta y = 1/3$.

a. Using the NVF-SMART scheme, applied via a deferred correction approach, discretize the equation over the computational domain and find the value of ϕ at each element centroid.
b. Using the TVD-SMART scheme, applied via a deferred correction approach, discretize the equation over the computational domain and find the value of ϕ at each element centroid.
c. Using the NVF-SUPERBEE applied via the NVF-NWF method setup the system of equations over the domain.
d. Using the TVD-MUSCL applied via the TVD-DWF method setup the system of equations over the domain.

Exercise 7

The advection of a step profile in an oblique velocity field, $\mathbf{v} = 2\mathbf{i} + \mathbf{j}$, shown in Fig. 12.24 is governed by

$$\nabla \cdot (\rho \mathbf{v} \phi) = 0$$

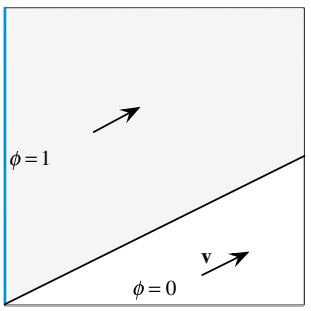

Fig. 12.24 Advection of a step profile in an oblique velocity field

For different grid sizes, setup the problem and solve it in OpenFOAM® and uFVM using the following HR advection schemes assuming unit dimensions in x and y directions, and compare results with the exact solution $(\rho = 1)$:

a. MINMOD
b. OSHER
c. SMART

Exercise 8
The Smith-Hutton test governed by

$$\nabla \cdot (\rho \mathbf{v} \phi) = 0$$

and illustrated in Fig. 12.25, involves the pure advection of a step profile in a rotational velocity field described as

$$\mathbf{v} = 2y\left(1 - x^2\right)\mathbf{i} - 2x\left(1 - y^2\right)\mathbf{j}$$

For different grid sizes, solve the test in OpenFOAM® and uFVM using the following advection schemes, and compare results with the exact solution $(\rho = 1)$:

a. Bounded CD
b. MUSCL
c. SUPERB

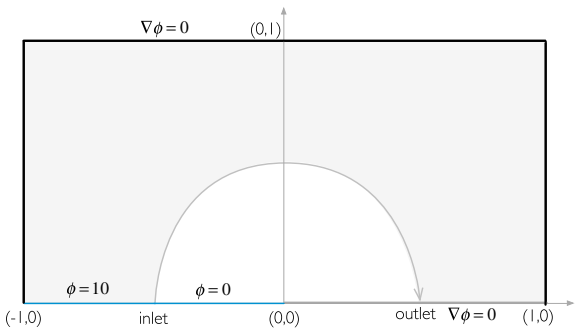

Fig. 12.25 Advection of a step profile in a two dimensional rotational velocity field

Exercise 9

a. Using Doxygen [34] list all the derived classes of the class limitedSurfaceInterpolationScheme<Type>.
b. Verify the correct implementation of the derived upwind<Type> class: check the weights function.
c. Find all OpenFOAM® limiter classes listed in Eq. (12.44) (vanLeerLimiter). Compare the formula with the OpenFOAM® implementation.

References

1. Leonard BP (1988) Universal limiter for transient interpolation modeling of the advective transport equations: the ULTIMATE conservative difference. NASA TR-100916, ICOMP-88-11
2. Leonard BP (1987) SHARP simulation of discontinuities in highly convective steady flow. NASA TM-100240
3. Leonard BP, Lock AP, MacVean MK (1995) Extended numerical integration for genuinely multidimensional advective transport insuring conservation. In: Proceedings of the ninth international conference numerical methods in laminar and turbulent flows, vol 9(1), pp 1–12
4. Gaskell PH, Lau AKC (1988) Curvature compensated convective transport: SMART, a new boundedness preserving transport algorithm. Int J Numer Meth Fluids 8(6):617–641
5. Godunov S, Ryabenki V (1963) Spectral stability criteria for boundary value problems for non self-adjoint difference equations. Uspekhi Mat Nauk 18:1–12
6. Fromm EA (1968) A method for reducing dispersion in convective difference schemes. J Comput Phys 3:176–189
7. Sheu TWH, Wang SK, Tsai SF (1998) Development of a high-resolution scheme for a multi-dimensional advection-diffusion equation. J Comput Phys 144(1):1–16
8. Leonard BP, Niknaffs HS (1991) Sharp monotonic resolution of discontinuities without clipping of narrow extrema. Comput Fluids 19:141–154
9. Van Leer B (1977) Towards the ultimate conservation difference scheme V. A second order sequel to Godunov's method. J Comput Phys 23:101–136
10. Zhu J, Rodi W (1991) A low-dispersion and bounded convection scheme. Comput Methods Appl Mech Eng 92:87–96
11. Yee HC, Warming RF, Harten A (1983) Implicit total variation diminishing (TVD) schemes for steady-state calculations. NASA Technical Memorandum 84832
12. Sweby PK (1984) High resolution schemes using flux limiters for hyperbolic conservation laws. SIAM J Numer Anal 21(5):995–1011
13. Chakravarth SR (1987) Development of upwind schemes for the Euler equations. NASA Contractor Report 4043
14. VanderHeyden WB, Kashiwa BA (1998) Compatible fluxes for Van Leer advection. J Comput Phys 146:1–28
15. Boris JP, Book DL (1973) Flux-corrected transport: I. SHASTA, a fluid transport algorithm that works. J Comput Phys 11:38–69
16. Kuzmin D, Turek S (2002) Flux correction tools for finite elements. J Comput Phys 175:525–558
17. Zalesak S (1979) Fully multidimensional flux corrected algorithm for fluid. J Comput Phys 31:335–362
18. Leonard BP (1988) Simple high-accuracy resolution program for convective modelling of discontinuities. Int J Numer Meth Eng 8:1291–1318
19. Spekreise S (1987) Multigrid solution of monotone second order discretizations of hyperbolic conservation laws. Math Comput 49(179):135–155
20. Barth T, Jespersen DC (1989) The design and application of upwind schemes on unstructured meshes. AIAA paper 89-0366
21. Leonard BP (1991) The ULTIMATE conservative difference scheme applied to unsteady one-dimensional advection. Comput Methods Appl Mech Eng 88(1):17–74
22. Dritschel DG, Fontane J (2010) The combined Lagrangian advection method. J Comput Phys 229:5408–5417
23. Leonard BP, MacVean MK, Lock AP (1993) Positivity-preserving numerical schemes for multidimensional advection. Technical Memorandum TM-106055 ICOMP-93-05, NASA
24. Leonard BP (1988) Simple high-accuracy resolution program for convective modelling of discontinuities. Int J Numer Meth Fluids 8:1291–1318

25. Leonard BP, Mokhtari S (1990) Beyond first-order upwinding: the ULTRA-SHARP alternative for non-oscillatory steady state simulation of convection. Int J Numer Methods Eng 30:729–766
26. Harten A (1983) High resolution schemes for hyperbolic conservation laws. J Comput Phys 49:357–393
27. Sweby PK (1984) High resolution schemes using flux limiters for hyperbolic conservation laws. SIAM J Numer Anal 21(5):995–1011
28. Van Leer B (1974) Towards the ultimate conservative difference scheme, 11. Monotonicity and conservation combined in a second order scheme. J Comput Phys 14:361–370
29. Darwish M, Moukalled F (1996) The normalized weighting factor method: a novel technique for accelerating the convergence of high-resolution convective schemes. Numer Heat Transf, Part B: Fundam 30:217–237
30. Osher S (1984) Shock modeling in transonic and supersonic flow. In: Habashi WG (ed) Recent advances in numerical methods in fluids, 4. Advances in computational transonics. Pineridge Press, Swansea
31. Darwish MS (1993) A new high-resolution scheme based on the normalized variable formulation. Numer Heat Transf, Part B: Fundam 24(3):353–371
32. OpenFOAM, 2015 Version 2.3.x. http://www.openfoam.org
33. Darwish M, Moukalled F (1994) Normalized variable and space formulation methodology for high-resolution schemes. Numer Heat Transf, Part B 26(1):79–96
34. OpenFOAM Doxygen, 2015 Version 2.3.x. http://www.openfoam.org/docs/cpp/